JOURNAL OF GEOPHYSICAL RESEARCH, VOL. 114, B12101, doi:10.1029/2009JB006604, 2009

The record of changing hematite and goethite accumulation over the past 22 Myr on the Chinese Loess Plateau from magnetic measurements and diffuse reflectance spectroscopy

Qingzhen Hao,[1,2] Frank Oldfield,[3] Jan Bloemendal,[3] José Torrent,[4] and Zhengtang Guo[1]

Received 10 May 2009; revised 7 August 2009; accepted 10 September 2009; published 23 December 2009.

[1] High-field isothermal remanence (HIRM) and diffuse reflectance spectroscopy (DRS) were used to characterize hematite and goethite in a suite of bulk and particle-sized fractioned samples from the Chinese Loess Plateau, representing the main changes in magnetic mineralogy over the past 22 Myr. The record of DRS-defined hematite largely reflects variations in the pedogenic fraction (<2 μm). By contrast, the detrital fraction (>8 μm) makes the main contribution to goethite concentrations in the bulk samples. Pedogenic goethite concentrations generally vary inversely with those of hematite. The lack of consistent correlations between HIRM-inferred mineral content and DRS measurements casts doubt on the validity of using HIRM to characterize the concentrations and relative proportions of hematite and goethite in sediments representing a long time span or a wide grain size distribution. The progressive decline in the coercivity of the antiferromagnetic minerals in bulk samples throughout the whole period is mainly an expression of changes in the detrital fraction, reflecting changes in the source region, possibly involving increased aluminum substitution. The good correlation between DRS-defined hematite and frequency-dependent magnetic susceptibility in several chronologically defined subgroups of samples is consistent with the hypothesis that maghemite forms a transitional phase in a weathering sequence from ferrihydrite to hematite. The results shed new light on using HIRM to characterize hematite and goethite in sediments and on the history of weathering and climate change over the past 22 Myr in the dust source regions and on the Loess Plateau.

Citation: Hao, Q., F. Oldfield, J. Bloemendal, J. Torrent, and Z. Guo (2009), The record of changing hematite and goethite accumulation over the past 22 Myr on the Chinese Loess Plateau from magnetic measurements and diffuse reflectance spectroscopy, *J. Geophys. Res.*, *114*, B12101, doi:10.1029/2009JB006604.

1. Introduction

[2] Since the pioneering studies of *Heller and Liu* [1984] magnetic measurements of loess sections from the Chinese Loess Plateau (CLP) have been used as a basis for reconstructing the history of climatic change in the region. Most of the research has been focused on sections spanning all or part of the Quaternary [e.g., *Heller and Evans*, 1995; *Maher and Thompson*, 1999; *Evans and Heller*, 2001; *Liu et al.*, 2007a, and references therein] and, to a lesser degree, the Pliocene [e.g., *X. Liu et al.*, 2003; *Nie et al.*, 2007]. Recent research, however, has drawn attention to the existence of loess profiles in the west of the CLP that provide a quasi-continuous record from the early Miocene onward, spanning the past 22 Myr [*Guo et al.*, 2002, 2008; *Hao and Guo*, 2007]. These profiles constitute one of the longest continental records of Neogene environmental change anywhere in the world, but before their magnetic properties can be interpreted in terms of their paleoenvironmental implications, they require careful and systematic evaluation.

[3] Although the magnetic properties of loess are almost universally dominated by the record of changing ferrimagnetic concentrations (magnetite and/or maghemite), the fact that most samples contain a significant hard remanence component points to the ubiquitous presence of imperfect antiferromagnetic minerals (hematite and/or goethite). In studies where the main concern is with the dominant magnetic carriers of either the rock magnetic or paleomagnetic signatures [e.g., *Zhou et al.*, 1990; *Maher and Thompson*, 1991; *Evans and Heller*, 1994; *Zhu et al.*, 1994; *Q. Liu et al.*, 2003; *Deng et al.*, 2004; *Bloemendal and Liu*, 2005; *Sartori et al.*, 2005], or where magnetic susceptibility measurements alone are used to infer past climate regimes [e.g., *An et al.*, 1991; *Maher*, 1998; *Chen et al.*, 1999; *Fang et al.*, 1999; *Hao and Guo*, 2005], this hard remanence component usually receives little attention. Where, however, the main aim is to use the magnetic properties of the

[1]Key Laboratory of Cenozoic Geology and Environment, Institute of Geology and Geophysics, Chinese Academy of Sciences, Beijing, China.
[2]Also at Department of Geography, University of Liverpool, Liverpool, UK.
[3]Department of Geography, University of Liverpool, Liverpool, UK.
[4]Departamento de Ciencias y Recursos Agrícolas y Forestales, Universidad de Córdoba, Campus de Rabanales, Córdoba, Spain.

0148-0227/09/2009JB006604$09.00

samples to contribute to a greater understanding of the changing weathering and hence climatic regimes experienced, both in the source regions of the loess and at the point of deposition, the hard remanence components become of prime importance. Routine magnetic measurements, whether of susceptibility or remanence, inevitably underestimate their contribution to the magnetic mineralogy of the sample since these antiferromagnetic minerals give rise to susceptibility and remanence values per unit mass between two and three orders of magnitude less than those generated by the ferrimagnetic minerals [*Peters and Dekkers*, 2003].

[4] The present paper considers the evidence for changing contributions of hematite and goethite to the magnetic minerals recorded in loess spanning the past 22 Myr. The samples analyzed are the ones previously selected to represent the main changes in magnetic mineralogy over the past 22 Myr and already used in previous publications [*Hao et al.*, 2008a, 2008b]. The first of these papers summarizes the results of magnetic measurements based on bulk samples, the second presents a basis for differentiating between, and separately characterizing the pedogenic and detrital fractions of each sample, using pipette analysis to provide particle-sized subsamples. The ferrimagnetic component of the particle-sized subsamples was considered briefly in both *Hao et al.* [2008b] and *Oldfield et al.* [2009]. In the present article we present evidence derived from diffuse reflectance spectroscopy (DRS), increasingly used to reconstruct hematite and goethite concentrations [*Ji et al.*, 2001; *Balsam et al.*, 2004; *Torrent and Barrón*, 2003; *Torrent et al.*, 2006, 2007] and high-field isothermal remanence (HIRM) measurements on both bulk samples and particle-sized subsamples. Our overriding aim is to establish the changing contribution of hematite and goethite to the magnetic mineralogy of the bulk samples and both the pedogenic and detrital components. We also compare the results obtained from DRS measurements with the HIRM often used as a basis for inferring the changing contributions of imperfect antiferromagnetic minerals to magnetic mineral assemblages.

2. Methods

2.1. Samples

[5] The thick eolian deposits of the late Cenozoic era in northern China comprise three formations. The uppermost comprises the well-known Quaternary loess-paleosol alternations spanning the past 2.6 Myr [*Liu*, 1985; *Kukla and An*, 1989], the complete sequences of which are mainly found in the eastern Loess Plateau. The sequence below the Holocene soil is subdivided into three major stratigraphic units from the bottom upward: Wucheng (2.6–1.26 Myr), Lishi (1.26–0.073 Myr), and Malan (0.073–0.011 Myr) [*Liu*, 1985; *Kukla and An*, 1989; *Ding et al.*, 2002]. Below these units lie the late Miocene-Pliocene eolian deposits found both in the eastern and western Loess Plateau region. In the eastern region, the Hipparion Red-Earth Formation (also called Red Clay) of ~8–6 Myr to 2.6 Myr conformably underlies the Quaternary loess-paleosol sequences [*Ding et al.*, 1998; *Sun et al.*, 1998]. On the basis of macro- and micromorphology, sedimentological evidence from the Xifeng Red-Earth section and spatial correlations, *Guo et al.* [2001] suggest that the formation of typical loess-paleosol alternations was started at 3.6 Myr at Xifeng. Prior to this, the eolian deposits in the middle part were affected by groundwater oscillations, and below this, by alluvial and slope processes. In the western Loess Plateau, however, the newly recorded Dongwan section shows much clearer alternations of loess and paleosol horizons which are also characterized by magnetic susceptibility fluctuations with a much higher amplitude than in the eastern sites [*Hao and Guo*, 2004]. These features are also confirmed by a newly dated section in the western Qinling Mts [*Ge and Guo*, 2008]. The third and earliest formation comprises the Miocene loess-paleosol sequences from the western Loess Plateau, with the most complete sequence QA-I covering 22–6.2 Myr [e.g., *Guo et al.*, 2002; *Lu et al.*, 2004; *Liu et al.*, 2005; *Hao and Guo*, 2007; *Guo et al.*, 2008].

[6] The samples come from three sites: Xifeng (XF, 0–3.4 Myr), Dongwan (DW, 3.5–7 Myr), and Qinan (QA-I, 6.2–22 Myr), respectively (Figure 1). DW and the QA-I section are recently discovered Neogene loess-soil sequences in the western CLP [*Guo et al.*, 2002; *Hao and Guo*, 2004]. Since there are no well-preserved loess sections postdating 3.6 Myr from the western part of the CLP close to the DW and QA-I sections, samples dating from post 3.6 Myr come from the well-documented XF section, 210 km to the east [*Sun et al.*, 1998; *Guo et al.*, 1998, 2001]. We analyzed 53 bulk samples and particle-sized subsamples of 26 of the bulk samples. Wherever possible, samples are selected from adjacent loess/paleosol couplets.

2.2. Diffuse Reflectance Spectroscopy

[7] The DRS technique provides a quantitative method to determine the mass concentrations of hematite and goethite. It has been successfully used in marine deposits [*Balsam and Deaton*, 1991] and loess sections from the CLP [*Ji et al.*, 2001; *Balsam et al.*, 2004; *Torrent et al.*, 2006, 2007].

[8] In this study, we measured the hematite and goethite content of 53 bulk samples and 52 particle-sized separates (26 clay fraction and 26 coarse fraction). The DRS of fine powdered samples (<10 μm) was recorded from 380 to 900 nm in 0.5 nm steps at a scan rate of 30 nm min^{-1}, using a Varian Cary 1E spectrophotometer equipped with a $BaSO_4$-coated integrating sphere 73 mm in diameter (Varian Inc., Palo Alto, California). The samples were pressed by hand into the hole of 8 × 17 mm rectangular white plastic holders (thickness 2.5 mm) at a pressure >500 kPa. The second derivative spectrum of the Kubelka-Munk (K-M) remission function at each wavelength was calculated according to *Torrent and Barrón* [2003]. The intensities of the bands at ~425 nm (I_{425}) and ~535 nm (I_{535}), which are proportional to the concentration of goethite and hematite, respectively [*Scheinost et al.*, 1998], can thus be used as proxies for relative changes in the mass concentration of goethite and hematite. The mass ratios of hematite to goethite are calculated by the calibration curve,

$$Y = -0.133 + 2.871X - 1.709X^2 \quad (1)$$

(where Y is the Hm/(Hm + Gt) mass ratio and X is the $I_{535}/(I_{425} + I_{535})$ ratio). This calibration curve was based on 22 soil samples from the Mediterranean region and the "true" concentration of the two minerals was quantitatively determined using X-ray diffraction. The equation accounted

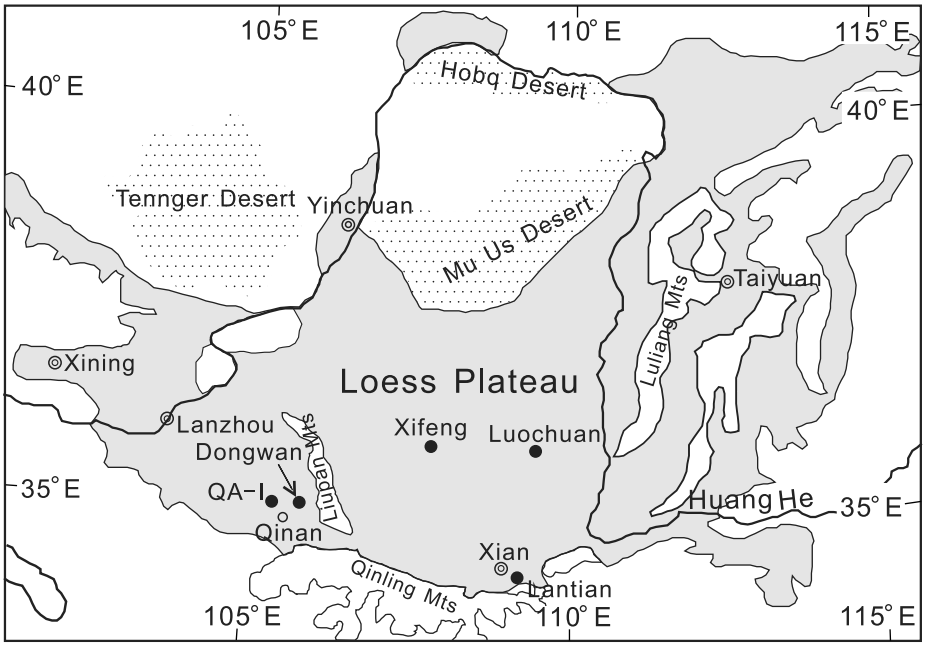

Figure 1. Map showing the Loess Plateau and the location of the site mentioned.

for 90% of the variance in Y and held at $0.07 < X < 0.4$, a condition which was fulfilled by our loess and paleosol samples. The absolute concentrations of hematite and goethite were estimated by assigning all of the citrate-bicarbonate-dithionite-extractable Fe (Fed) to these two minerals, and the contribution of ferrihydrite and pedogenic ferrimagnetic minerals to Fed are neglected due to their low mass percentage [*Torrent et al.*, 2007],

$$\mathrm{Fed} = \mathrm{Hm}/1.43 + \mathrm{Gt}/1.59. \quad (2)$$

Fed was determined by the method of *Mehra and Jackson* [1960], and was used to evaluate the iron liberated from the silicate minerals by weathering. The concentrations of hematite and goethite were calculated from above two equations.

2.3. Magnetic Measurements

[9] The magnetic identification of imperfect antiferromagnetic minerals in natural material is often difficult at room temperature owing to their weak magnetic signals relative to those of ferrimagnetic minerals. In the traditional HIRM acquisition experiments, the viscous remanent magnetization of ferrimagnetic minerals represents an important source of error for measurements in applied fields above 1 T. In recent years, the introduction of alternating field (AF) demagnetization into the HIRM experiment efficiently removes the influence of ferrimagnetic minerals and increases the signal-to-noise ratio. Although the continued acquisition of IRM at fields above 0.3 T has been observed for ferrimagnetic minerals [e.g., *Liu et al.*, 2002; *Maher et al.*, 2004], the IRM resulting from the presence of these ferrimagnetic minerals can be fully removed by AF demagnetisation with the peak values of 100 mT, 120 mT or 200 mT [*Larrasoana et al.*, 2003; *Maher et al.*, 2004; *Carter-Stiglitz et al.*, 2006; *Deng et al.*, 2006].

[10] In this study, we conducted HIRM acquisition experiments on 26 bulk samples as well as on the clay (<2 μm) and coarse (>8 μm) fractions separated from these samples, as described in the following section. Around 300 mg of each sample was tightly pressed into a plastic tube, and then magnetized stepwise at 20 steps for the 26 bulk samples and 22 steps for their particle separates, applying DC fields ranging from 0.2 T to 7 T, generated by an MMPM 5 Pulse Magnetizer. After each acquisition step, the samples were subjected to AF demagnetization with a peak value of 200 mT, using a DTECH AF demagnetizer. The residual IRM after this treatment was measured on a Molspin spinner magnetometer with a noise level of 0.1×10^{-8} Am^2. The residual HIRM represents the signal reflecting the presence of hematite and/or goethite.

[11] We have developed a modification of the L ratio proposed by *Liu et al.* [2007b] designed to investigate the coercivity of antiferrimagnetic minerals [*Hao et al.*, 2008a]. The original L ratio was defined as the ratio of two remanences after AF field demagnetization of an IRM imparted in a 1 T field with a peak AF of 100 mT and 300 mT: $\mathrm{IRM_{AF@300mT}}/\mathrm{IRM_{AF@100mT}}$. Our modified L ratio was based on "Hard" IRMs obtained by DC demagnetization: $\mathrm{Hard_{300mT}}/\mathrm{Hard_{100mT}}$, where $\mathrm{Hard_{100mT}}$ and $\mathrm{Hard_{300}}$mT refer to the part of SIRM, imparted in the field of 1 T, that remains unreversed after applications of −100 mT and −300 mT, respectively. Calculations were made as follows: $\mathrm{Hard_{100mT}} = (\mathrm{SIRM} + \mathrm{IRM_{-100mT}})/2$, $\mathrm{Hard_{300mT}} = (\mathrm{SIRM} + \mathrm{IRM_{-300mT}})/2$. The modified L ratio, $\mathrm{Hard_{300mT}}/\mathrm{Hard_{100mT}}$, shows a close correlation with original L ratio obtained by AF methods for both soils and loess samples [*Hao et al.*, 2008a, Figure 10], and provides an effective method for recording the coercivity changes of antiferrimagnetic minerals in Chinese eolian deposits using DC demagnetization.

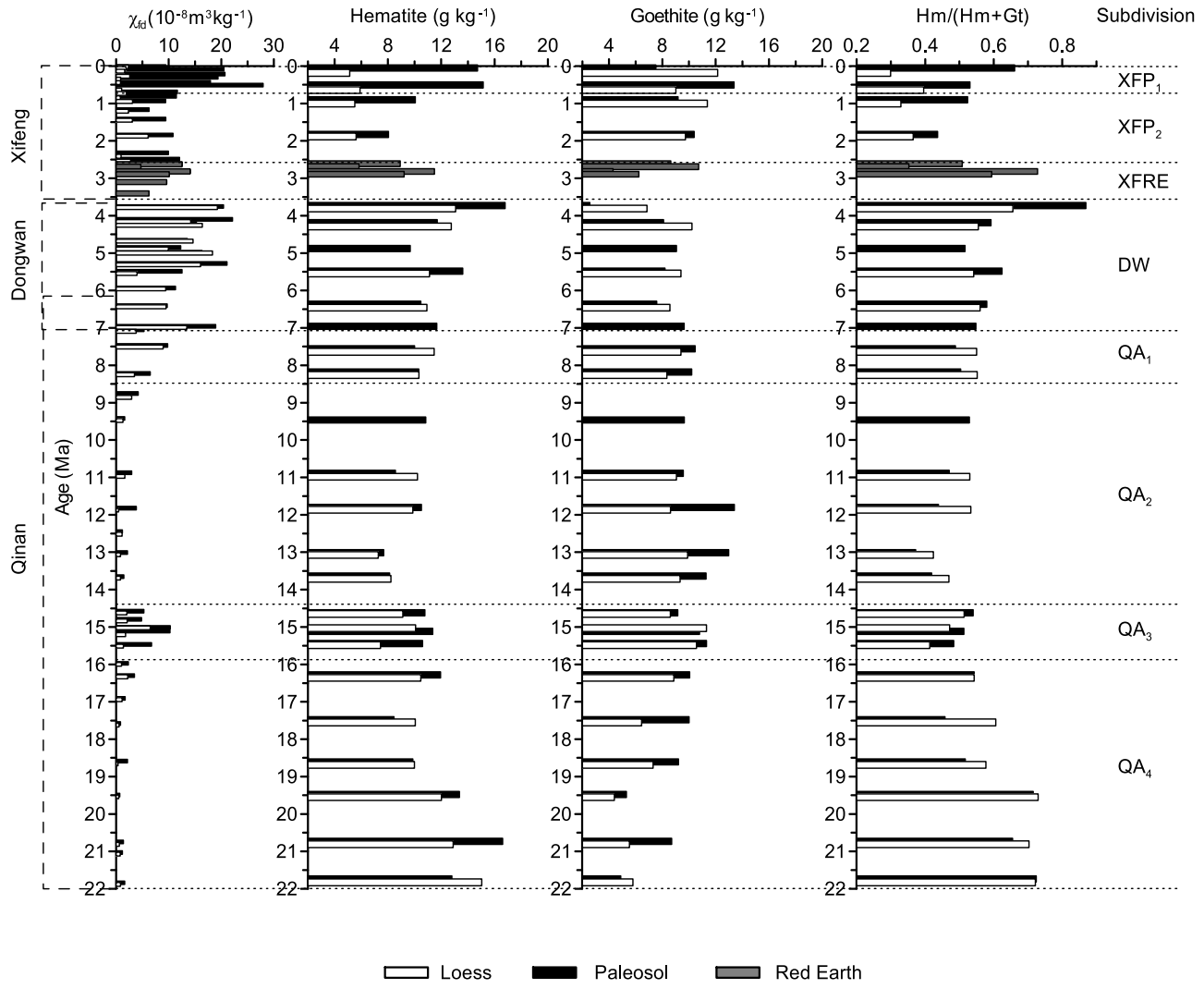

Figure 2. Diffuse reflectance spectroscopy (DRS)-derived concentrations and quotients of hematite and goethite in bulk samples of eolian deposits from the Chinese Loess Plateau spanning the past 22 Myr. (left) Changes in frequency-dependent magnetic susceptibility [*Hao et al.*, 2008a], χ_{fd}, in the past 22 Myr, which is often used as an indicator of ferrimagnetic enhancement due to pedogenic processes. All the results are calculated on a carbonate-free basis. (right) Eight sample groups defined by routine magnetic properties [*Hao et al.*, 2008a].

2.4. Particle Fractionation

[12] All of the 26 bulk samples in the HIRM experiments were separated by the pipette method into four grain-sized fractions: <2 μm, 2–4 μm, 4–8 μm and >8 μm [*Hao et al.*, 2008b]. First, ~100 g of each bulk sample was split into three subsamples and put into 200 mL beakers; excessive buffered acetic acid (2M, pH 4.5) was added to remove the carbonate [e.g., *Freeman*, 1986]. The pretest on 10 bulk samples confirmed that the acetic acid treatment led to a loss of ferrimagnetic signals of less than 3% and loss of hard remanence signals of less than 9%. The reaction time generally varied from 24 to 48 hours. The samples were then rinsed and transferred into a conical flask and shaken on a reciprocating shaker for 24 hours after adding 25 mL 0.05 M Calgon solution. The subsequent particle separation was similar to the procedures detailed by *Zheng et al.* [1991]. The pipetted subsamples were freeze-dried to avoid any oxidation of iron minerals. The low contribution of material >63 μm in all but the youngest Pleistocene loess rendered it unnecessary for present purposes to sieve the samples prior to pipette analysis. Our previous research demonstrates that the <2 μm and >8 μm fractions can be used to represent the pedogenic and detrital fractions, respectively, and these two fractions accounts for 73.5%–90.6% (80.1 ± 4.2%, n = 26) of the bulk samples [*Hao et al.*, 2008b].

3. Results

[13] Figures 2–5 present the results of the DRS analyses calculated on a carbonate-free basis. In Figure 2, the results of the DRS analysis on bulk samples are plotted against the chronology, established using paleomagnetic reversals as age controls for the XF (Red Earth), DW and QA-I sections [*Sun et al.*, 1998; *Guo et al.*, 2002; *Hao and Guo*, 2004],

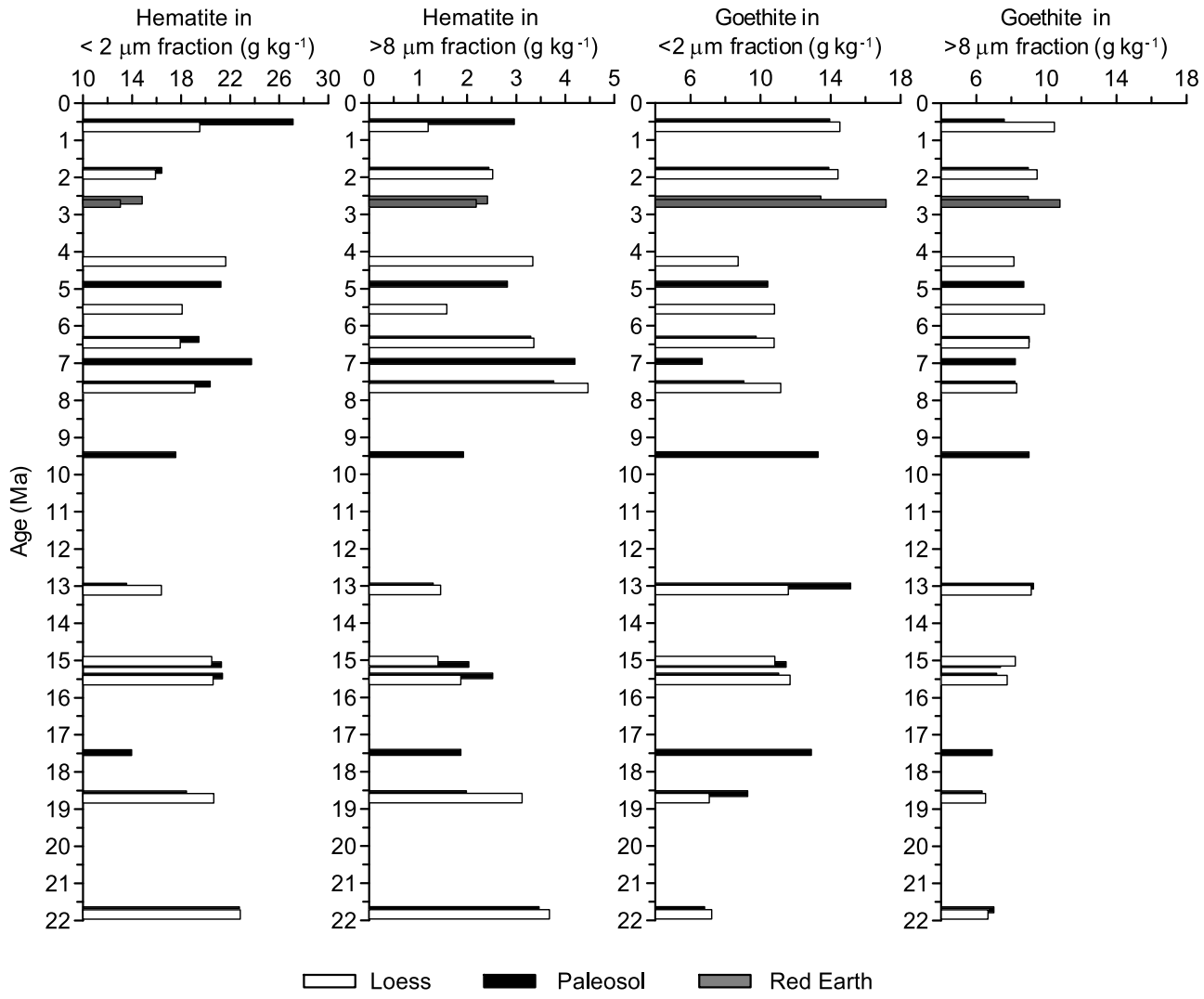

Figure 3. DRS-derived concentrations of hematite and goethite in <2 μm and >8 μm fractions of selected samples in eolian deposits over the past 22 Myr on the Chinese Loess Plateau.

Interpolation between dated polarity boundaries was made using Kukla's magnetic susceptibility age model [*Kukla et al.*, 1990]. Although the premise upon which this model is based is no longer accepted, it nevertheless provides a reasonable basis for generating an age model that allows for the differences in rates of accumulation between loess and paleosols. The chronology for the youngest part of the sequence was established by comparison with the generally accepted XF time scale [*Kukla et al.*, 1990]. The results of the DRS analyses are set against the graph for mass specific frequency-dependent susceptibility (χ_{fd}), the difference between low-frequency and high-frequency magnetic susceptibility in the low field, since this is a commonly used indicator of pedogenic development in studies of Quaternary loess [e.g., *Zhou et al.*, 1990; *Liu et al.*, 2004]. The subdivisions down the right hand side of the graph are those defined by *Hao et al.* [2008a] on the basis of routine magnetic measurements. The following features may be noted (Figure 2).

[14] 1. In the most recent part of the record, representing the period when glacial/interglacial cycles occurred with a 100 kyr periodicity, hematite is more abundant in the paleosols than in the intervening loess layers and the contrast in goethite concentrations between the paleosols and loess is variable.

[15] 2. In the earlier Pleistocene samples, hematite is once more relatively more abundant in the paleosols, but goethite generally shows higher concentrations than hematite in both the loess and paleosol layers.

[16] 3. In the pre-Pleistocene samples, there is no consistent difference in hematite concentrations between the loess and paleosol samples, save during the mid-Miocene period (QA_3) around 15 Myr when hematite concentrations were consistently higher in the paleosols.

[17] 4. Goethite concentrations in the DW section (7–3.6 Myr) are generally higher in the loess layers than in the paleosols, but in most of the earlier samples, in the QA-I section, the opposite is the case. The sole exception is in the QA_3 part of the record where goethite concentrations show little difference between loess and paleosols.

[18] 5. Hematite as a proportion of the combined total varies between 0.30 and 0.87, with the widest variations in the Plio-Pleistocene part of the record where loess gives rise to minima and vice versa. Prior to this, the proportions are

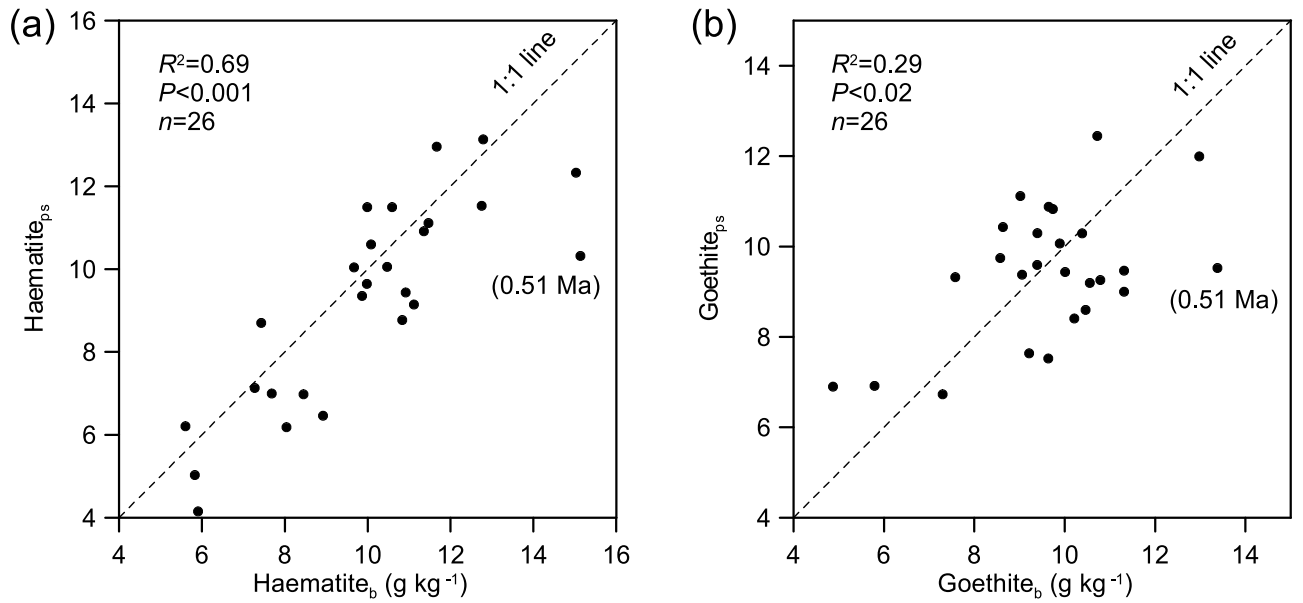

Figure 4. Correlation between the DRS-derived bulk concentrations (hematite$_b$ and goethite$_b$) and the concentrations estimated from the particle size–based measurements (hematite$_{ps}$ and goethite$_{ps}$). All concentrations are on a carbonate-free basis.

more stable with minimum values around 12–14 Myr and maxima before 19 Myr.

[19] 6. The basal loess-paleosol couplet, just postdating 22 Myr, is almost the only one in which both hematite and goethite show significantly higher values in the loess.

[20] In Figure 3, the results of DRS analyses are shown on a mass specific basis for particle sized subsamples representative of the pedogenic (<2 μm) and detrital (>8 μm) portions of the 26 samples subjected to disaggregation, carbonate removal and pipette analysis. The main features are as follows.

[21] 1. Throughout the whole of the sequence hematite concentrations in the pedogenic fraction are around an order of magnitude higher than in the detrital fraction. Moreover, there is a tendency for concentrations in the latter to roughly parallel those in the former, suggesting the possibility of imperfect separation during pipetting.

[22] 2. Only in the topmost sample is there a strong difference in hematite concentration between the paleosol and loess members of the couplet.

[23] 3. Goethite concentrations are broadly similar in the two fractions with usually a higher concentration in the clay fraction. Whereas they are generally less than the hematite concentrations in the <2 μm fraction, they consistently exceed them in the >8 μm fraction.

[24] In several previous articles [*Zheng et al.*, 1991; *Chen et al.*, 1995], measurements of the magnetic properties of each particle-sized fraction and the mass proportion of that fraction were used to calculate the contribution that size fraction made to each magnetic measurement in the bulk sample. In the present case, particle size–based DRS measurements were only made on the two extreme size fractions which together made up the bulk of the sample mass in each case [*Hao et al.*, 2008b]. In order to assess the degree of validity of contribution estimates made for the two particle size subsamples we first plot for both hematite and goethite, the relationship between the measured bulk concentration and the concentration estimated by ascribing the values for the <2 μm subsample to the 2–4 μm subsample and the values for the >8 μm subsample to the 4–8 μm subsample. As the graphs show (Figure 4) the correlation is quite good, with very few significant outliers.

[25] Figure 5 shows, for both hematite and goethite, the contribution made by the <2 μm and >8 μm size fractions to the bulk values for each sample. Once the mass contribution of each particle-sized subsample is taken into account, the clay/pedogenic fraction still makes the dominant contribution to the bulk hematite values in all cases, but the difference between the two is much less. Goethite contributions from the coarser fraction often exceed those from the fine fraction, especially in the late Plio-Pleistocene part of the sequence.

[26] Figures 6 and 7 present the results of the high field isothermal remanence measurements. All are plotted on a carbonate-free basis. The values represent stepwise IRM acquisition followed by AF demagnetization with a peak field of 200 mT at each step. HIRM$_{1.5T}$ and HIRM$_{4T}$ (residual HIRM imparted in field of 1.5 and 4 T, respectively) are likely to be largely dominated by a hematite contribution [*Heller*, 1978; *France and Oldfield*, 2000; *Maher et al.*, 2004]. Acquisition beyond this (HIRM$_{7-4T}$, the difference between residual HIRM imparted in fields of 4 and 7 T, respectively) is likely to reflect the contribution from goethite [*Walden et al.*, 1999; *France and Oldfield*, 2000; *Maher et al.*, 2004].

[27] In the bulk sample measurements (Figure 6), inferred hematite contributions vary little between paired loess and paleosol samples irrespective of the field used. Both show lower values in samples predating 15 Myr. The pattern in the HIRM$_{7T}$ trace parallels those at lower fields as indeed does the sequence of values for HIRM$_{7-4T}$, the likely indicator of a goethite contribution. The last two columns may be taken as representing the putative hematite and goethite contributions to the remanence measured at the

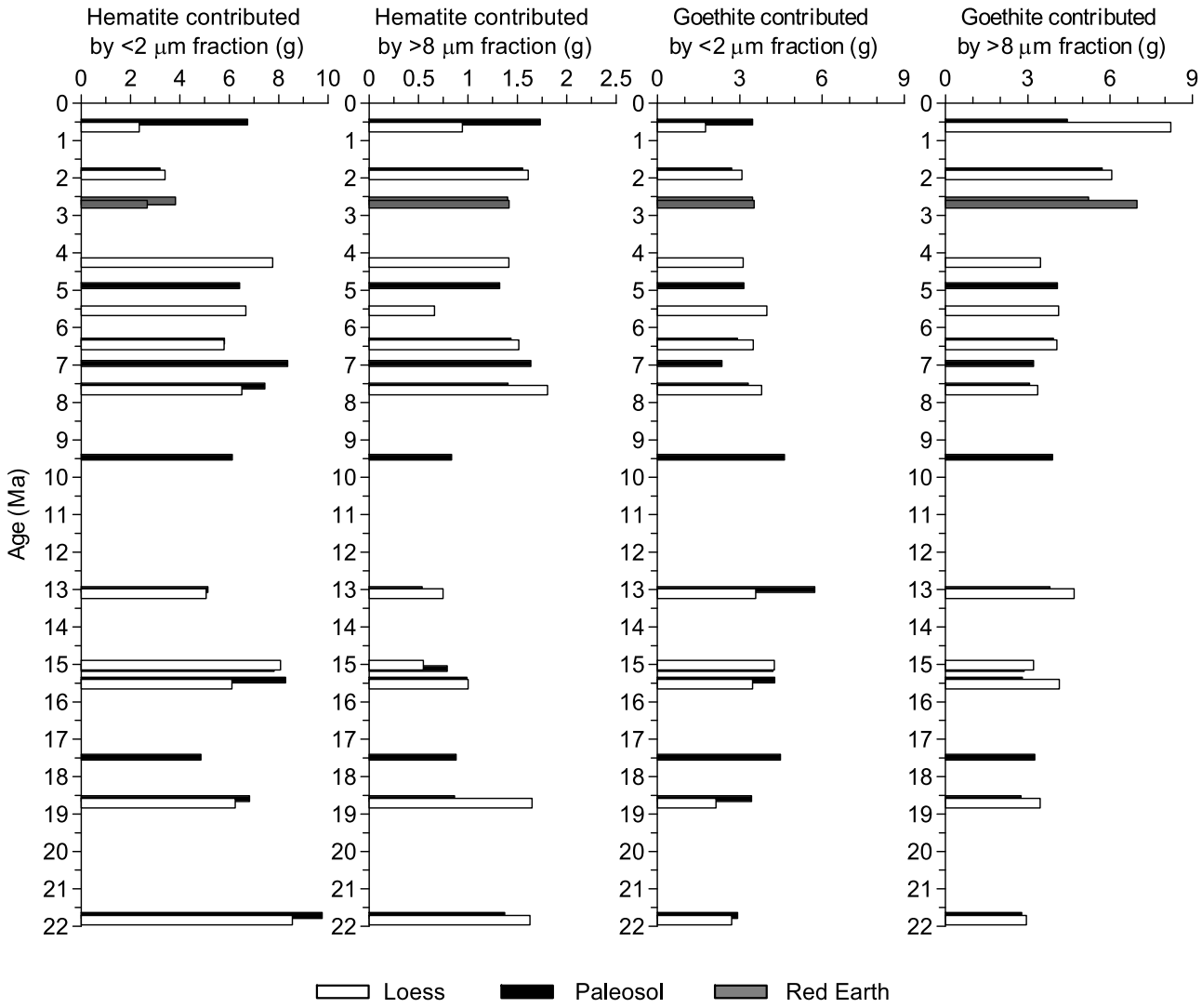

Figure 5. Calculated total contribution of fractions <2 μm and >8 μm to the DRS-derived hematite and goethite content of 1000 g bulk samples of loess and paleosols over the past 22 Myr.

highest available field, respectively. The results as a whole demonstrate that very little remanence is acquired above 4 T.

[28] Figure 7 gives the same range of data for the <2 μm (Figure 7a) and >8 μm (Figure 7b) particle-sized fractions. In both graphs, the same contrast between inferred hematite and goethite contributions is evident. "Hematite" is, overall, more or less equally well represented in each size fraction though the reduced values in the bulk samples pre–15 Myr are paralleled in the >8 μm fraction but not in the clays. Hematite values tend to be higher in the paleosols than in the adjacent loess samples.

[29] Figure 8 confirms the consistency between the measured bulk values for the different high-field remanence components and the same values calculated from the particle size based measurements, using the same procedure as outlined for Figure 4.

4. Discussion

4.1. Changing Hematite and Goethite Contributions

[30] Here, we use the DRS-based estimates as the least ambiguous indicators of the changing concentrations of both hematite and goethite. The particle size–based measurements, by confirming the extent to which hematite is concentrated in the finest fraction throughout the whole sequence reinforce the tendency in the bulk measurements for values to be higher in the paleosols than in the adjacent loess layers, in agreement with the findings of, e.g., *Balsam et al.* [2004] for the post 2.6 Myr interval at Luochuan and Lingtai. It follows that, on the basis of the DRS measurements, most of the hematite in the loess samples is pedogenic. A smaller, though still significant component is in the detrital fraction, though this may, to some degree, reflect imperfect particle separation. Some fine hematite in coatings on quartz grains may also be present in the coarse fraction. The contrast between higher paleosol and lower loess concentrations is at its strongest in the Pleistocene samples, especially those postdating the shift to 100 ka periodicity. This may, in part at least, reflect the relative thickness of the loess. In the most recent sections, the thick loess layers include a large depth range of minimally weathered material. By contrast, the Pliocene and Miocene loess layers are much thinner, mostly less than 1 m, and are much more likely to have any initial detrital signature

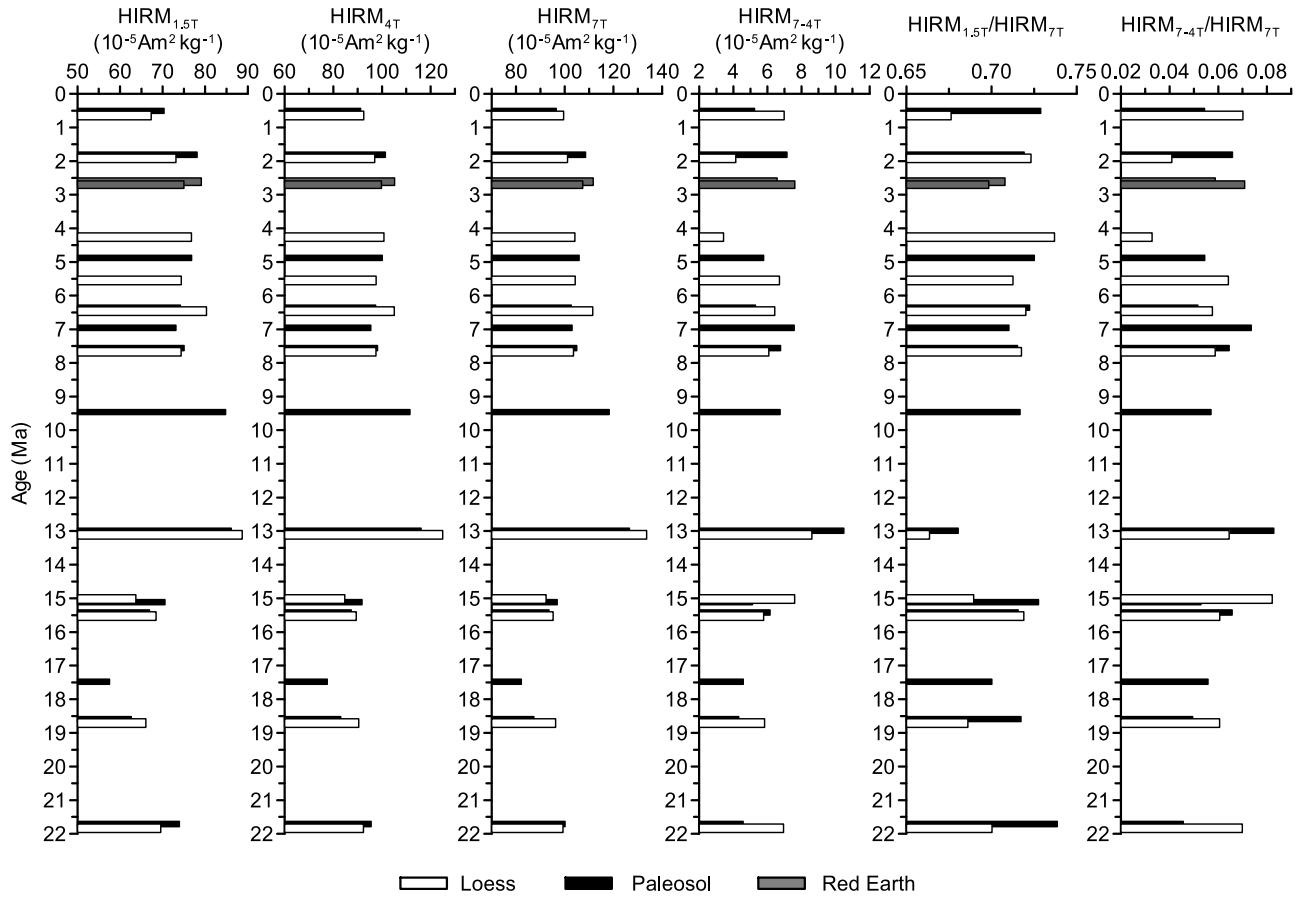

Figure 6. Measurements of high-field isothermal remanent magnetization (HIRM), imparted in fields of 1.5 T, 4 T, and 7 T, and calculations based on these for bulk loess and paleosol samples over the past 22 Myr. The HIRM data are residual values following alternating field (AF) demagnetization after imparting the IRM in each field. All are calculated on a carbonate-free basis.

partially modified by weathering throughout the whole depth of each loess/paleosol couplet. Magnetic weathering signatures, notably increased hard remanence values, persist throughout these depths in warm temperate, subhumid soil profiles on sedimentary bedrock [e.g., *Oldfield*, 1991]. The greater degree of carbonate translocation in these pre-Pleistocene loess layers [*Hao et al.*, 2008a] is also consistent with this interpretation. The indication that hematite in loess sequences is dominantly pedogenic is in good agreement with the inferences in several recent publications [*Torrent et al.*, 2006, 2007]. Pedogenic hematite concentrations vary by a factor of two, with a maximum in the late Pleistocene paleosol and mimima in the earlier Pleistocene and around 17.5 Myr in the Miocene (Figure 3).

[31] Goethite, by contrast, generally appears to be roughly equally concentrated in both the pedogenic and detrital fractions. The fact that the latter form a higher percentage of the bulk sample means that the dominant goethite contribution appears to be generated in the source area prior to transport and deposition [*Torrent et al.*, 2006, 2007]. Geochemical studies [*Gallet et al.*, 1996; *Gu et al.*, 1997; *Liang et al.*, 2009] are consistent with the view that the sources of loess throughout the whole period of deposition include weathered material. The overall tendency for the detrital goethite to increase in concentration throughout the whole record might indicate progressive weathering in the source areas (Figure 3). There is a tendency for pedogenic goethite concentrations to vary inversely with those of hematite. Provided this is not an analytical artifact, this may give a pointer to variations in weathering regime on the Loess Plateau.

4.2. Indications From High-Field Remanence Measurements

[32] Several factors should be borne in mind in considering HIRM as potential indicators of variations in hematite and goethite concentrations. First, there is no convincing way of converting the values used into absolute concentrations, even if uniformity of coercivity can be assumed within each mineral type. Second, this assumption itself would be difficult to uphold in a data set that includes material spanning 22 Myr of accumulation and representing both primary deposition and pedogenesis. Whereas some proportionality between hard remanence characteristics and hematite concentrations may be a reasonable assumption in a confined system over a relatively short time interval, for example as by *Oldfield et al.* [2003], *Liu et al.* [2007b] show that this assumption breaks down with variations in such factors as hematite grain size and the degree of aluminum substitution. A further source of uncertainty is introduced by the small differences in high-field acquisition values in many cases, leading to a high degree of uncer-

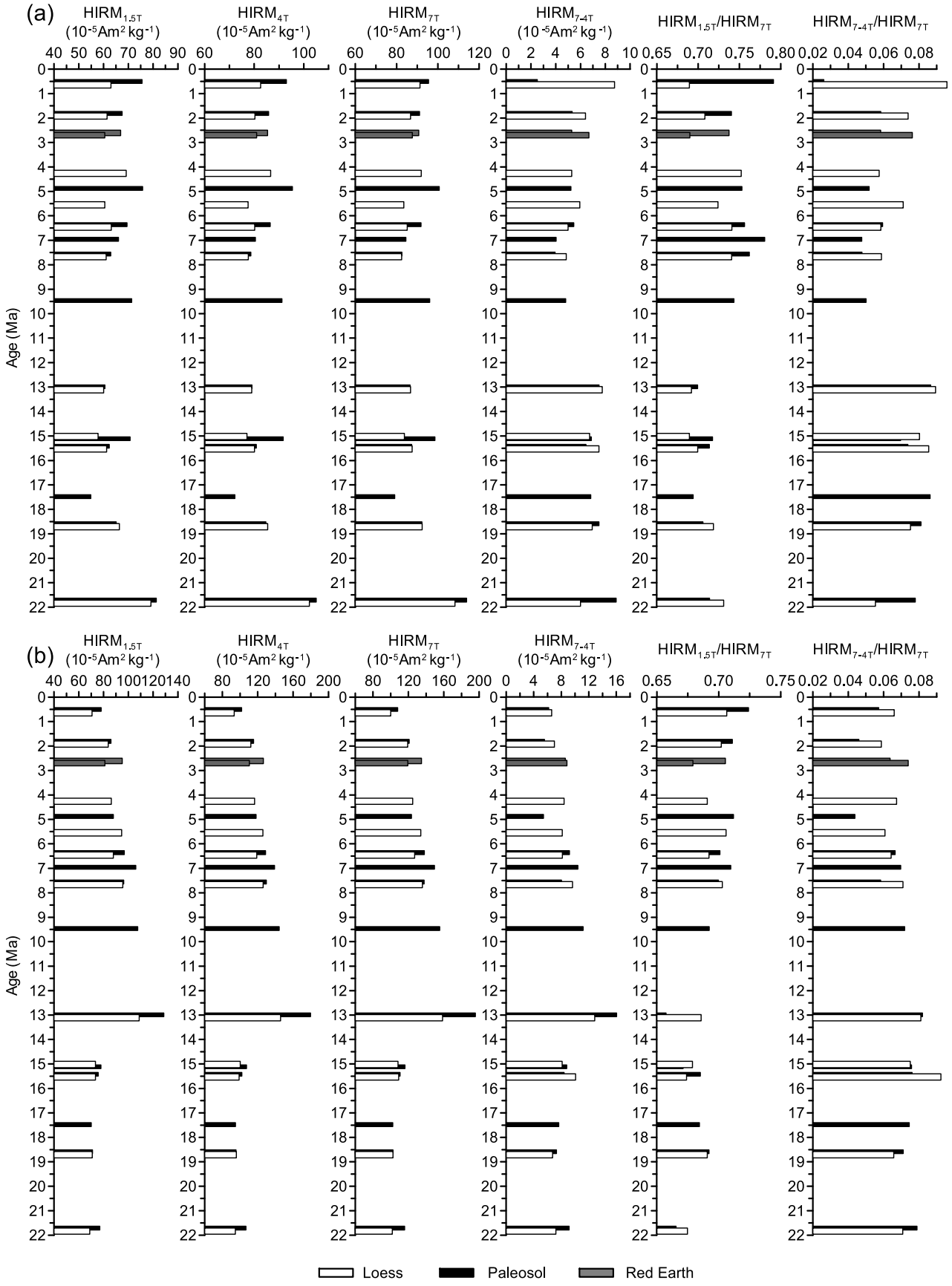

Figure 7. Measurements of HIRM, imparted in fields of 1.5 T, 4 T, and 7 T, and calculations based on these for the (a) <2 μm fractions and (b) >8 μm fractions. The HIRM data are residual values following AF demagnetization after imparting the IRM in each field.

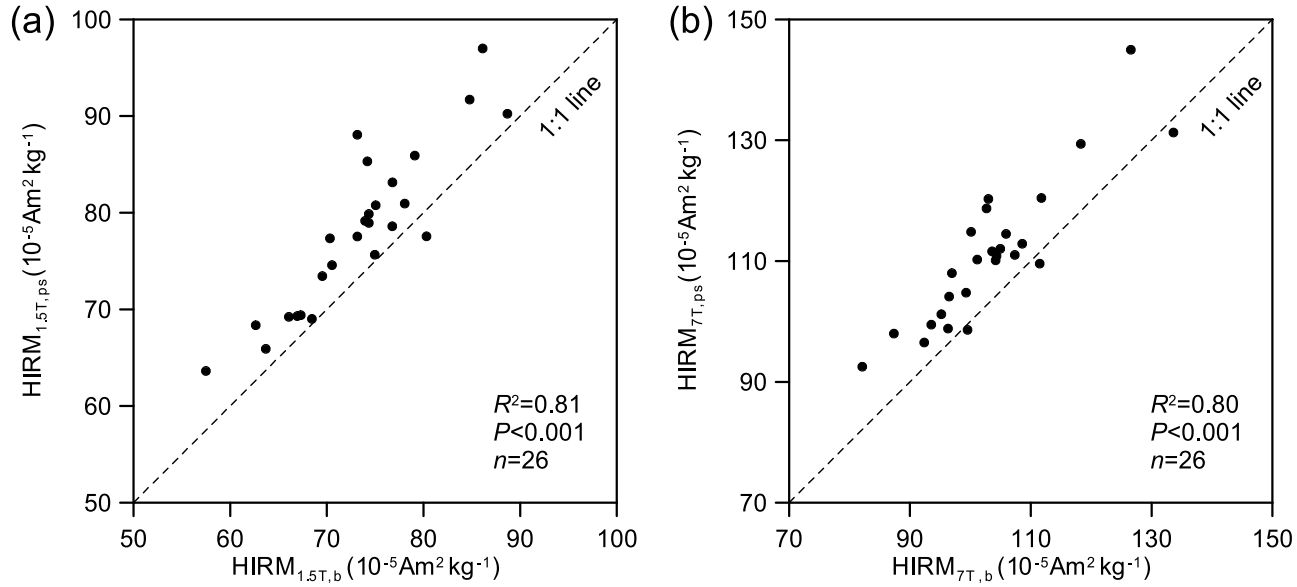

Figure 8. Correlation between the measured bulk HIRM values ($HIRM_{1.5T,\ b}$ and $HIRM_{7T,\ b}$) and the estimated ones based on the particle size measurements ($HIRM_{1.5T,\ ps}$ and $HIRM_{7T,\ ps}$). All measurements are calculated on a carbonate-free basis.

tainty in individual estimates based on simple subtraction [*Liu et al.*, 2002]. The problems involved in estimating changing goethite concentrations from HIRM are even more severe, not least because in many cases, goethite is known to acquire most of its remanence at even higher fields than those available for use in the present study [e.g., *Dekkers*, 1989]. Even where great care is taken to confirm and isolate a goethite component using orthogonal demagnetization and translation balance (Neel temperature) experiments, the results fall short of any approach to quantitative estimates [*France and Oldfield*, 2000]. The present results mostly reinforce the above reservations. For example, from the magnetic measurements, there is no indication of the contrast between hematite in the pedogenic and detrital components (Figure 7), that is clearly demonstrated in the DRS analyses (Figure 3). Moreover, there is no convincing parallel between the relative proportions of the two minerals inferred from the two methods.

[33] Figures 9 and 10 explore the extent to which, despite the above observations, there are parts of the record for which there is greater correlativity between the two sets of results.

[34] In Figure 9, carbonate-free "bulk" sample measurements are shown and the symbols are used to distinguish between three groups according to age. In all cases, the horizontal axis gives the results of the DRS analyses. Figures 9a and 9b show no significant relationships between the high-field magnetic properties and the DRS-determined mineral concentrations to which they may be expected to relate. Figures 9c and 9d compare magnetically derived and DRS-based quotients and, again, no clear relationships emerge.

[35] Figure 10 presents the same comparisons, but in this case, on a particle size–specific basis, with the results for the clay fraction on the left hand side and those for the coarse fraction on the right. In some cases, two, in others three separate time spans are identified by separate symbols. Figures 10a and 10b show moderately good correlations between the magnetic and DRS indicators for hematite ($R^2 = 0.38$, $P < 0.02$ for clay fractions and $R^2 = 0.40$, $P < 0.02$ for coarse fractions, $n = 14$) in the samples postdating 7.6 Myr. Earlier samples show a moderate correlation (<2 μm fraction, $R^2 = 0.41$, $P < 0.05$, $n = 12$) or an absence of correlation (>8 μm fraction). In the case of goethite (Figures 10c and 10d), the situation is rather different. There is a significant correlation only for the post 7.6 Myr samples in the clay fraction ($R^2 = 0.20$, $P > 0.1$, $n = 14$; $R^2 = 0.61$, $P < 0.01$, $n = 12$ (excluding the topmost two samples formed around 0.5–0.6 Myr)), but only for the samples older than 15 Myr in the >8 μm fraction ($R^2 = 0.42$, $P < 0.05$, $n = 9$). Figure 10e referring to the clay fractions, shows the only strong correlation between magnetic and DRS quotient values, but with different slopes, for the <7.6 Myr and >9.4 Myr sample sets. Overall, the particle size–based comparisons show more correlativity between magnetic and DRS-based results than do the bulk sample measurements and more correlations are in the clay fraction plots than in those from the coarse fractions. However, this overlooks one major anomaly, namely that the inferred hematite concentrations from the magnetic measurements are broadly comparable in the two particle size fractions whereas they differ by almost an order of magnitude in the DRS measurements. This is difficult to understand without raising the possibility that the latter technique may register hematite concentrations differently depending on particle size.

4.3. The Basis for the *L* Ratio Trends Through Time

[36] *Hao et al.* [2008a] establish a good correlation between the modified *L* ratio based on DC demagnetization results and the original ratio used by *Liu et al.* [2007b] to demonstrate, among other things, the fallibility of HIRM, notably the HIRM or *S* values (here called $Hard_{100mT}$ and $Hard_{300mT}$, respectively), as proxies for hematite concen-

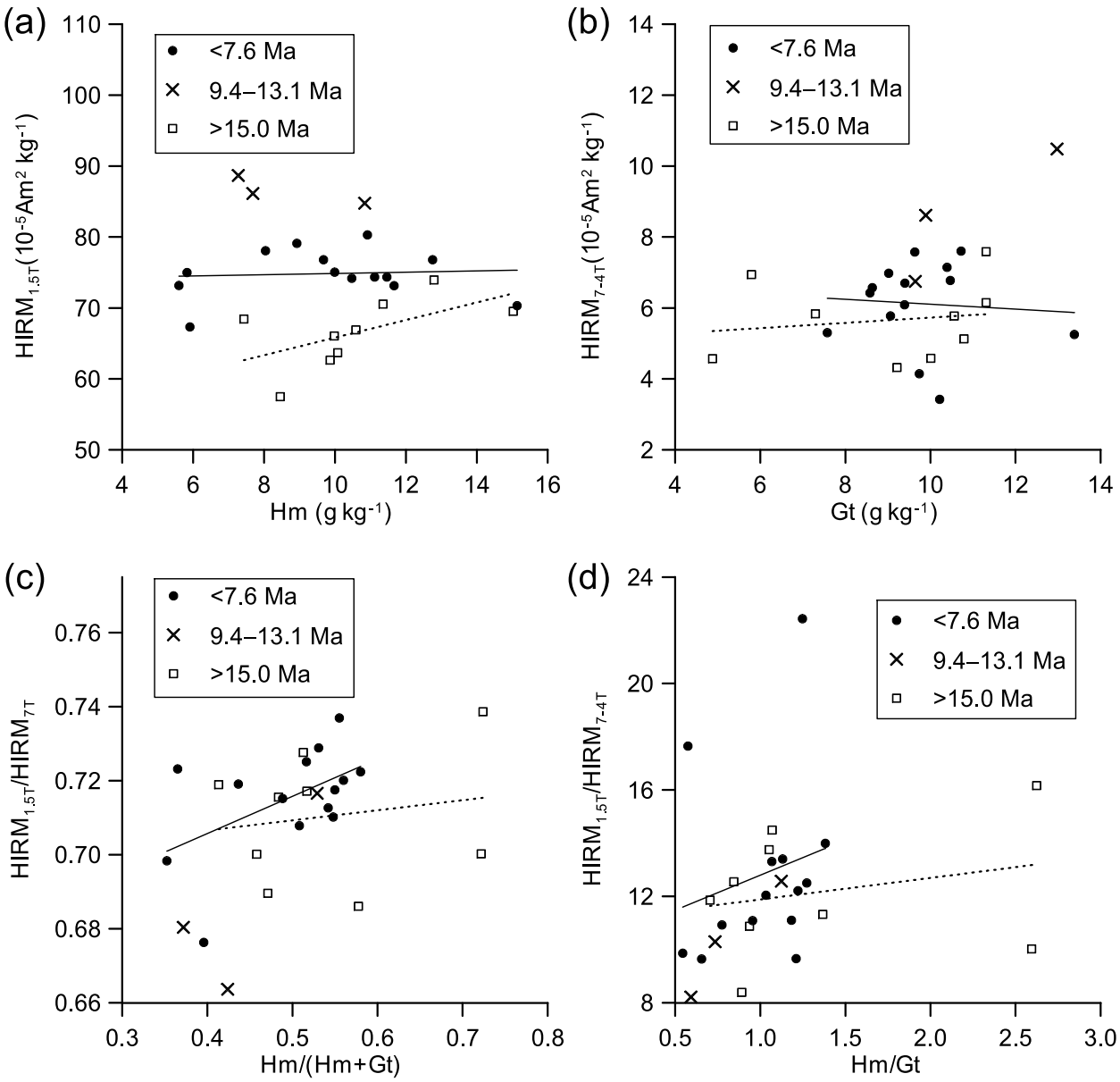

Figure 9. Cross-plot of DRS-defined concentrations and quotient values for hematite (Hm) and goethite (Gt) versus HIRM-inferred mineral concentrations and quotients in subgroups of the bulk loess and paleosol samples over the past 22 Myr. All data are calculated on a carbonate-free basis. The solid and dotted lines are the linear fit lines for the sample groups <7.6 Myr and >15.0 Myr, respectively.

trations [*Thompson and Oldfield*, 1986; *Bloemendal et al.*, 1992]. Figure 11 shows the trend in modified L ($Hard_{300mT}$/$Hard_{100mT}$) alongside the values for hard remanence using 100 mT and 300 mT as the discriminating fields. Several factors contribute to the problems that *Liu et al.* [2007b] identify, including differing degrees of aluminum substitution. The $Hard_{100mT}$ value may also be affected by the presence of high-coercivity maghemite, but in the present case, this is not likely to make a significant contribution to the trends, since the steepest changes in L, which are in the Quaternary part of the sequence, are common both to maghemite-poor loess and maghemite-rich paleosol samples. Since the former are the least-weathered sediments with some of the lowest ferrimagnetic concentrations in the whole record, maghemite is most unlikely to make a significant contribution to the trends recorded.

[37] Since some goethites can also begin to acquire remanence at fields between 100 mT and 1 T [e.g., *France and Oldfield*, 2000; *Maher et al.*, 2004], it is quite possible that changing goethite concentrations may contribute to the trend in L. In Figure 12, we compare the modified L ratio with the quotient giving the proportion of hematite to the sum of both hematite and goethite. Although there is a very general positive relationship, the R^2 value is low ($R^2 = 0.11$, $P < 0.02$, $n = 53$). However, this weak positive relationship runs contrary to the general concept that high Hm/(Hm + Gt) ratios mean a softer magnetic mineral assemblage. Within the set as a whole, no temporally defined subset of samples

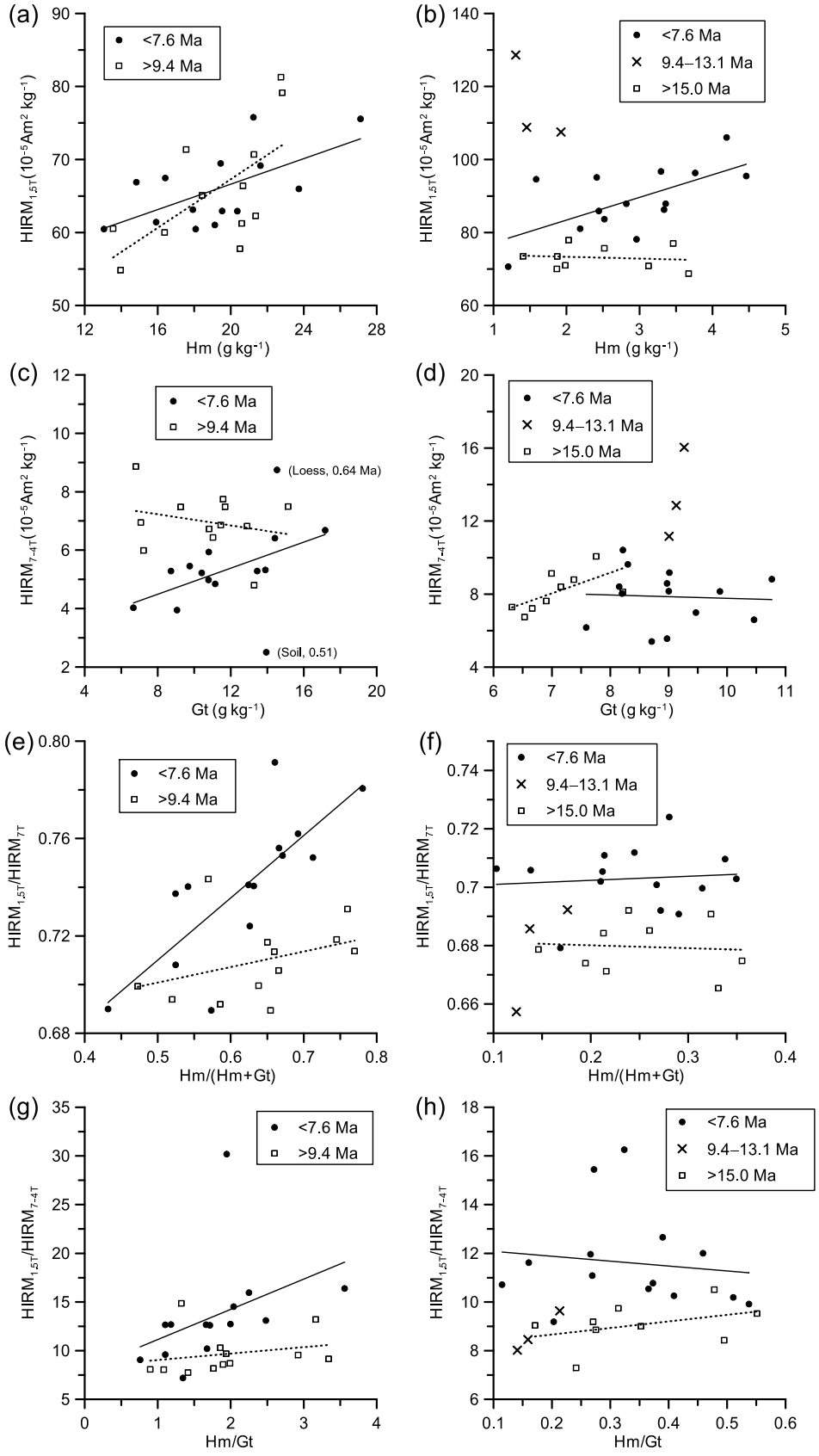

Figure 10. Cross-plot of DRS-defined concentrations and quotient values for hematite (Hm) and goethite (Gt) versus HIRM-inferred mineral concentrations and quotients in subgroups of the (left) <2 μm fraction and the (right) >8 μm fraction. The solid and dotted lines are the linear fit lines for the sample groups <7.6 Myr and >15.0 Myr, respectively.

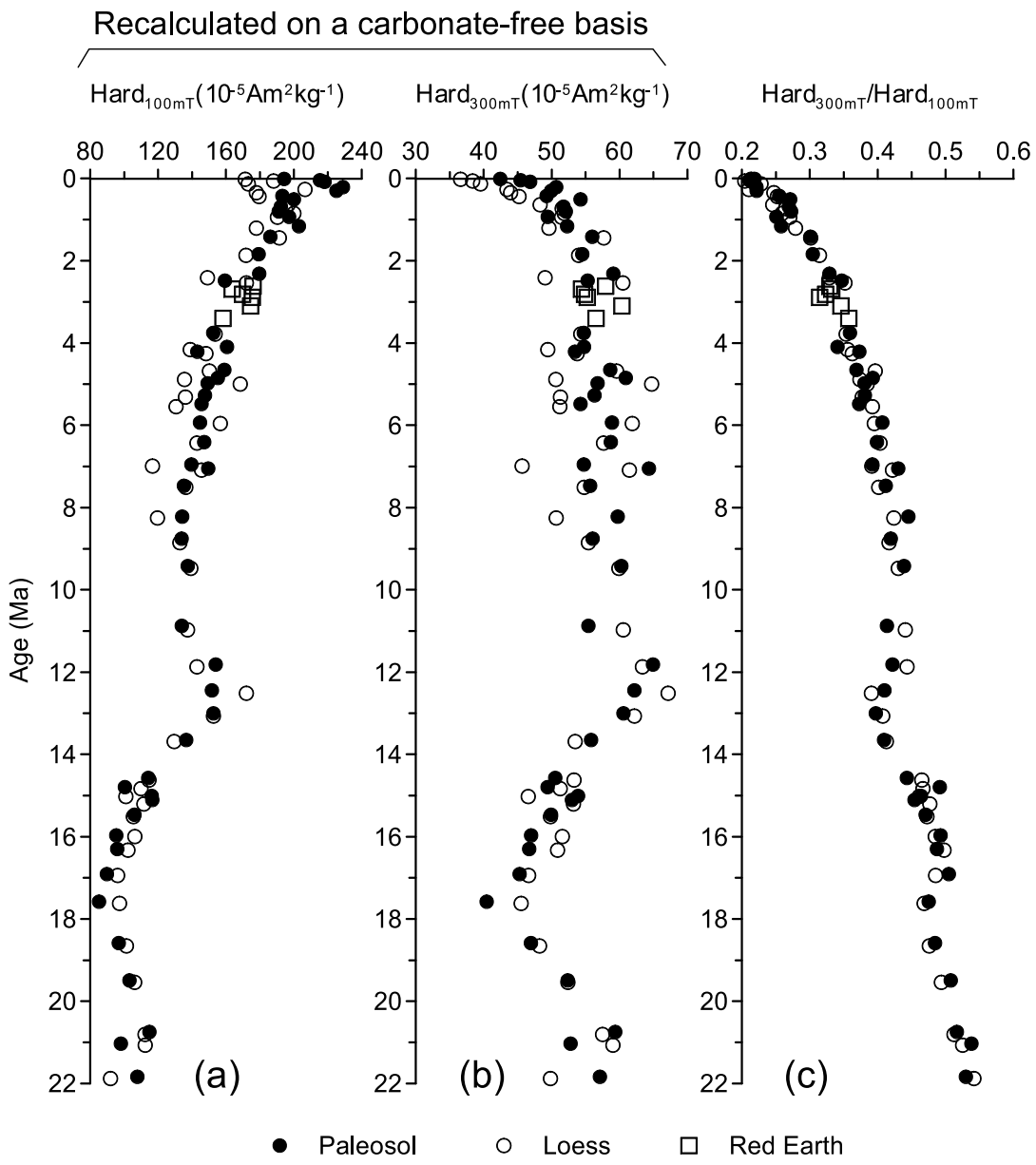

Figure 11. Hard IRMs ($Hard_{100mT}$ and $Hard_{300mT}$) and the revised L ratio ($Hard_{300mT}/Hard_{100mT}$) [*Liu et al.*, 2007b] for the bulk loess and paleosol samples over the past 22 Myr.

shows the expected negative relationship between L and the mineral quotient except for the samples (especially the paleosols) from the upper part of the XF profile. We conclude that the hematite:goethite ratio falls well short of explaining the full sequence of changes in the modified L ratio, but that it may contribute significantly to the trend in the most recent paleosols in the sequence.

[38] Magnetic grain size may be responsible for some of the trend, but this seems rather unlikely given the close links between magnetic grain size and particle size [*Oldfield et al.*, 2009] and the fact that magnetically fine-grained paleosols and coarse-grained loess layers both contribute equally to the trend. A further possibility is a progressive increase in aluminum substitution through time, interrupted only by the "kink" in the record between 14 and 12 Myr.

[39] One key question concerns the extent to which the trend reflects changes in the <2 μm pedogenic component or the >8 μm detrital component. Figure 13 shows that there is no clear parallel between the trends in L for the <2 μm fractions (Figure 13a) and the bulk samples (Figure 13c), there is a strong parallel between the trends in the coarse fraction (Figure 13b) and those in the bulk samples.

[40] From the above discussion, we infer that the trend in L reflects changes in the source material rather than in any in situ weathering products and that the source changes may include increased aluminum substitution. Whether these changes reflect trends in a single source region or a subtle shift in the balance between sources cannot be resolved from the present data. These relationships emerge despite the strong indications from the DRS analyses already

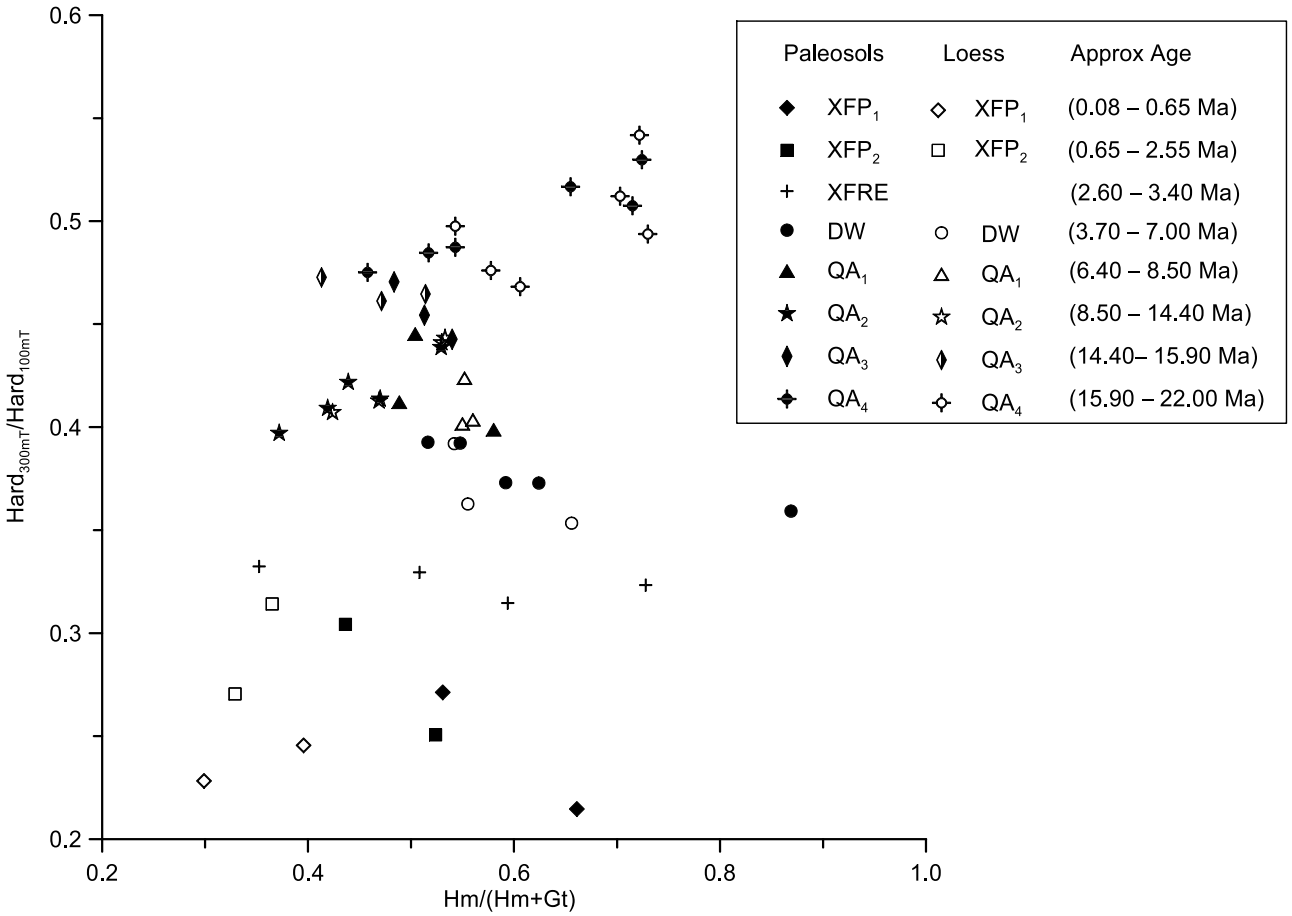

Figure 12. Cross-plot of Hm/(Hm + Gt) and the revised *L* ratio ($Hard_{300mT}/Hard_{100mT}$) in subgroups of the bulk eolian deposits over the past 22 Myr.

summarized above, that the hematite is mainly pedogenic in origin.

4.4. Hematite and Pedogenic Ferrimagnets

[41] Figure 14 plots DRS-determined hematite, considered to be dominantly pedogenic, against χ_{fd} values. The two graphs use separate symbols for age-defined subsets of samples. Figure 14a shows the results from the whole set of samples subjected to DRS analysis. Figure 14b expands the χ_{fd} scale and shows only the samples predating 8.3 Myr.

[42] There is a close correlation between DRS-defined hematite and χ_{fd} for the post 8.3 Myr sample set ($R^2 = 0.66$, $P < 0.001$, $n = 26$). The correlation is somewhat comparable ($R^2 = 0.78$, $P < 0.02$, $n = 6$) for the subset from 14.6 to 15.5 Myr, which corresponds to the mid-Miocene susceptibility peak in the QA-I profile; the slope is offset, but similar. The younger Miocene samples (9.4–13.7 Myr) show a much weaker correlation ($R^2 = 0.07$, $P > 0.1$, $n = 9$). The older Miocene samples (16.3–18.7 Myr) show a moderate correlation ($R^2 = 0.54$, $P < 0.1$, $n = 6$) again. Finally the oldest samples show a rather good correlation ($R^2 = 0.16$, $P > 0.1$, $n = 6$; $R^2 = 0.91$, $P < 0.02$, $n = 5$ (excluding one soil sample dated to 21.74 Myr)), with the steepest slope.

[43] Although the correlations between DRS-defined hematite and χ_{fd} do not prove the validity of the *Torrent et al.* [2006, 2007] hypothesis in which maghemite forms a transitional phase in a weathering sequence from ferrihydrite to hematite, this hypothesis would certainly provide the most economical explanation given the strong correlation over the past 8.3 Myr. If we adopt this as a working hypothesis, the weaker and finally absent relationship in much of the Miocene part of the sequence would point to more advanced weathering in which the progression to hematite became eventually almost complete. Whether this weathering took place in each case within the timeframe of the Earth orbitally driven loess and paleosol alternations, or reflects longer-term, supraorbital diagenesis cannot be established from the present data and remains, for the moment, an open question.

5. Conclusions

[44] 1. The results extend the findings of previous workers by providing the first evidence for changing hematite and goethite concentrations in loess-paleosol sequences that began to accumulate in the early Miocene; both the bulk samples and particle separates have been subjected to magnetic measurements and DRS. This provides a basis for evaluating the use of stepwise HIRM to quantitatively estimate the identity and concentrations of imperfect antiferromagnetic minerals.

[45] 2. Throughout the whole of the sequence of the past 22 Myr hematite concentrations in the pedogenic fraction

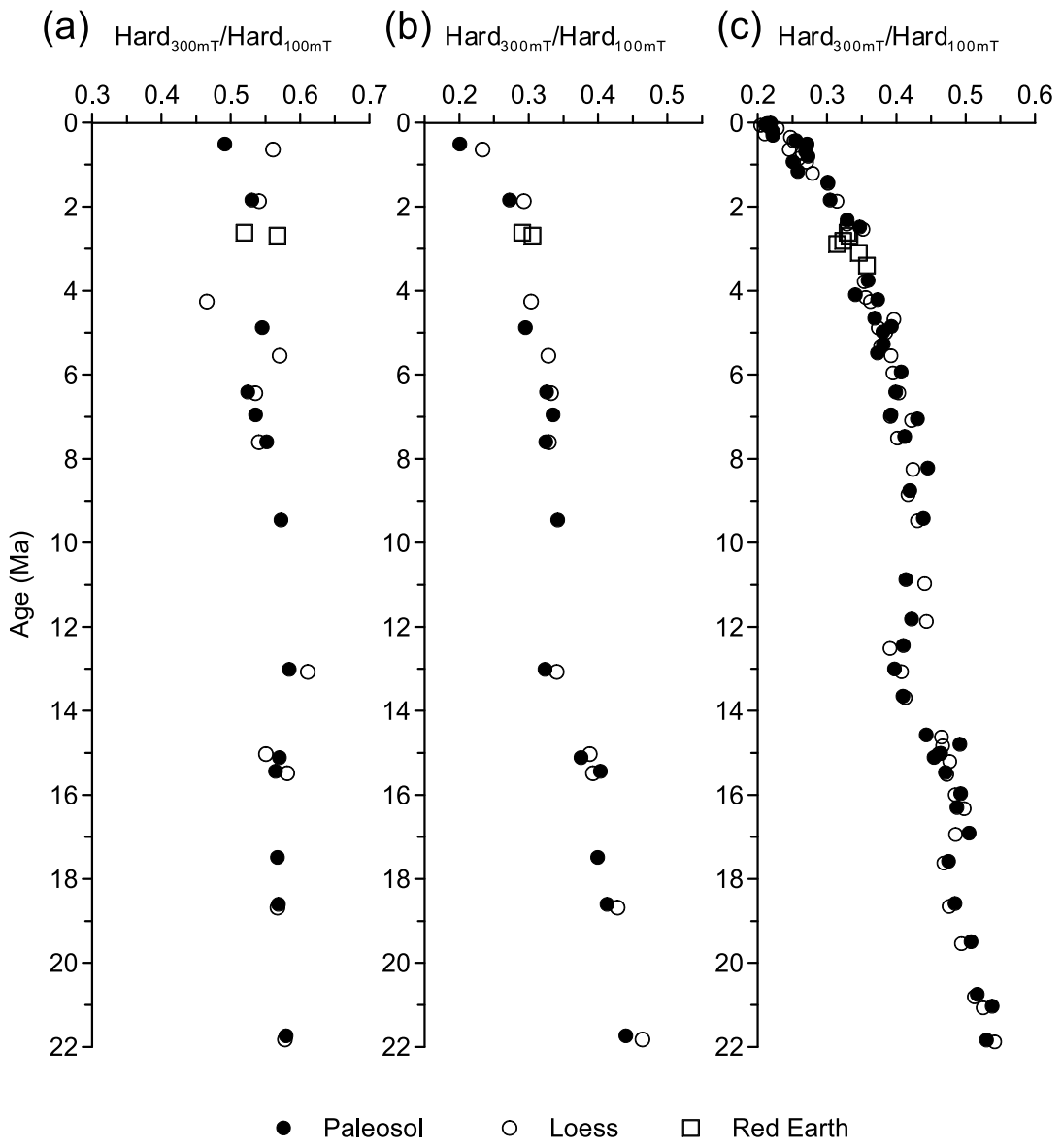

Figure 13. Comparison of the revised L ratio changes in the (a) <2 μm fraction, (b) >8 μm fraction, and (c) bulk samples.

(<2 μm) are around an order of magnitude higher than in the detrital fraction (>8 μm), consistent with the previous observation in the Pleistocene Chinese loess deposits that hematite is mainly pedogenic in origin. Goethite, by contrast, generally appears to be in roughly equal concentrations in both the pedogenic and detrital fractions. The higher contribution from the detrital fraction to the bulk samples indicates that the goethite record mainly reflects changes in the source area prior to transport and deposition. There is a tendency for pedogenic goethite concentrations to vary inversely with those of hematite.

[46] 3. There is very weak or no correlation between the HIRM-inferred mineral concentrations and quotients derived from these, and DRS measurement for both the bulk samples and for the detrital fraction. Moderate correlations between magnetic- and DRS-based inferences are generally present in the pedogenic fractions. This suggests that great caution must be used in applying the magnetic approach to characterizing hematite and goethite in sequences spanning a long period, or in samples sets spanning a wide range of grain sizes (e.g., from clay to coarse silt) if these minerals exist in both fine and coarse fractions.

[47] 4. On the basis of the comparisons between the DRS and HIRM measurements (Figure 10), there is a shift in the nature of both the hematite and goethite present in the pedogenic fraction around 9.4–13.1 Myr; shifts in the detrital fraction occur around 13.1–15 Myr and 7.6–9.4 Myr. These changes must be related to environmental changes in the Loess Plateau and dust source areas, and should be explored further in the future studies.

[48] 5. The DRS-estimated hematite:goethite ratio falls well short of explaining the decrease in the coercivity of imperfect antiferromagnetic minerals over the full sequences of the past 22 Myr. The parallel changes between the coarse fraction (>8 μm) and the bulk samples suggest that the imperfect ferromagnetic minerals in the coarse fraction are

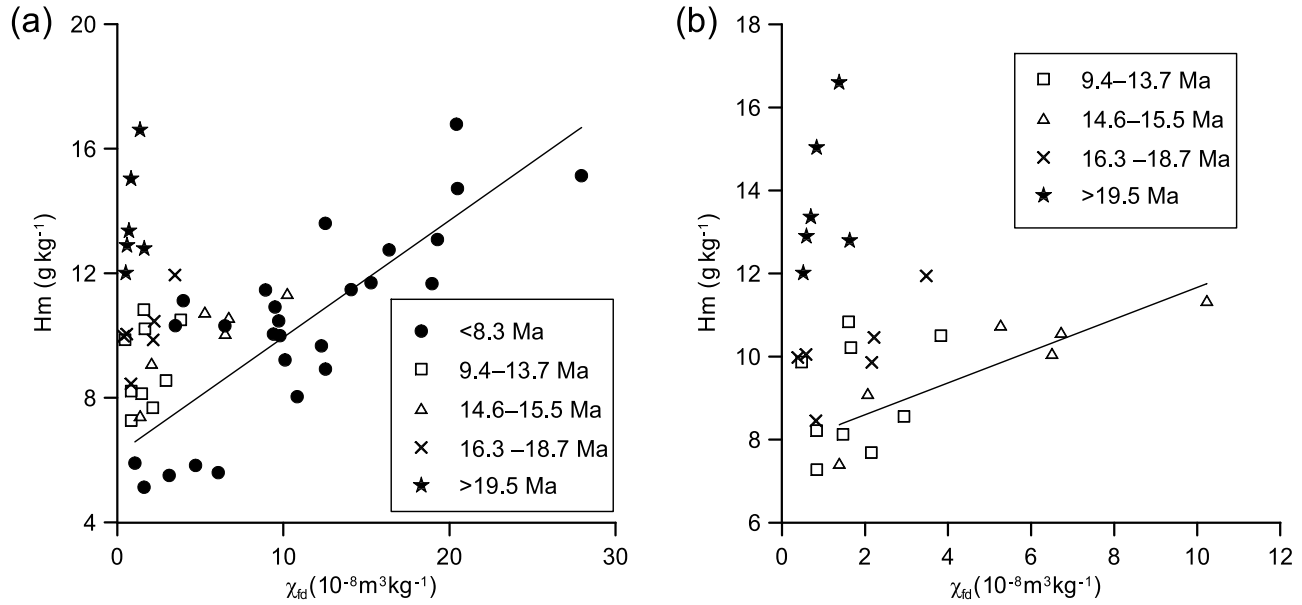

Figure 14. Cross-plots of (a) DRS-defined hematite versus frequency-dependent magnetic susceptibility, χ_{fd}, for the selected bulk samples over the past 22 Myr and (b) the expanded version of Figure 14a for samples predating 9.4 Myr.

responsible for the decreasing trend in L values in the bulk samples from the early Miocene onward. We infer that the trend in L reflects changes in the source material rather than in in situ weathering products and that the source changes may include increased aluminum substitution with increasing age.

[49] 6. The strong correlation between DRS-defined hematite and frequency-dependent magnetic susceptibility, χ_{fd}, over the past 8.3 Myr supports the *Torrent et al.* [2006] hypothesis whereby maghemite forms a transitional phase in a weathering sequence from ferrihydrite to hematite. The increased slope of the relationship in the Miocene part of the sequence (except for the high-susceptibility interval from 14.4 to 15.6 Myr) may point to more advanced weathering in which the progression to hematite became eventually almost complete. This possibility requires further study, as does the question of whether the weathering recorded reflects changes during a single Earth orbital cycle or longer-term diagenesis.

[50] **Acknowledgments.** This study was supported by the Chinese Academy of Sciences (KZCX2-YW-117) and the National Natural Science Foundation of China (projects 40672115 and 40730104). J.B. and Q.H. thank the Royal Society for financial support. Q.H. thanks Qingsong Liu for the helpful discussion during his short visit to Liverpool. We thank R. Jude for help with the magnetic measurements and A. Henderson, I. Cooper, and H. Hull for help with particle separation.

References

An, Z.-S., G. J. Kukla, S. C. Porter, and J. Xiao (1991), Magnetic susceptibility evidence of monsoon variation on the Loess Plateau of central China during the last 130,000 years, *Quat. Res.*, *36*, 29–36, doi:10.1016/0033-5894(91)90015-W.

Balsam, W. L., and B. C. Deaton (1991), Sediment dispersal in the Atlantic Ocean—evaluation by visible-light spectra, *Rev. Aquat. Sci.*, *4*, 411–447.

Balsam, W., J. F. Ji, and J. Chen (2004), Climatic interpretation of the Luochuan and Lingtai loess sections, China, based on changing iron oxide mineralogy and magnetic susceptibility, *Earth Planet. Sci. Lett.*, *223*, 335–348, doi:10.1016/j.epsl.2004.04.023.

Bloemendal, J., and X. M. Liu (2005), Rock magnetism and geochemistry of two plio-pleistocene Chinese loess-palaeosol sequences—implications for quantitative palaeoprecipitation reconstruction, *Palaeogeogr. Palaeoclimatol. Palaeoecol.*, *226*, 149–166, doi:10.1016/j.palaeo.2005.05.008.

Bloemendal, J., J. W. King, F. R. Hall, and S.-J. Doh (1992), Rock magnetism of Late Neogene and Pleistocene deep-sea sediments: Relationship to sediment source, diagenetic processes, and sediment lithology, *J. Geophys. Res.*, *97*, 4361–4375, doi:10.1029/91JB03068.

Carter-Stiglitz, B., S. K. Banerjee, A. Gourlan, and E. Oches (2006), A multi-proxy study of Argentina loess: Marine oxygen isotope stage 4 and 5 environmental record from pedogenic hematite, *Palaeogeogr. Palaeoclimatol. Palaeoecol.*, *239*, 45–62, doi:10.1016/j.palaeo.2006.01.008.

Chen, F., R. Wu, D. Pompei, and F. Oldfield (1995), Magnetic property and particle size variations in the late Pleistocene and Holocene parts of the Dadongling loess section near Xining, *Quat. Proc.*, *4*, 27–40.

Chen, F. H., J. Bloemendal, Z. D. Feng, J. M. Wang, E. Parker, and Z. T. Guo (1999), East Asian monsoon variations during oxygen isotope stage 5: Evidence from the northwestern margin of the Chinese Loess Plateau, *Quat. Sci. Rev.*, *18*, 1127–1135, doi:10.1016/S0277-3791(98)00047-X.

Dekkers, M. J. (1989), Magnetic properties of natural goethite—I. Grain-size dependence of some low- and high-field related rock magnetic parameters measured at room temperature, *Geophys. J.*, *97*, 323–340, doi:10.1111/j.1365-246X.1989.tb00504.x.

Deng, C., R. Zhu, K. L. Verosub, M. J. Singer, and N. J. Vidic (2004), Mineral magnetic properties of loess/paleosol couplets of the central Loess Plateau of China over the last 1.2 Myr, *J. Geophys. Res.*, *109*, B01103, doi:10.1029/2003JB002532.

Deng, C., J. Shaw, Q. Liu, Y. Pan, and R. Zhu (2006), Mineral magnetic variation of the Jingbian loess/paleosol sequence in the northern Loess Plateau of China: Implications for Quaternary development of Asian aridification and cooling, *Earth Planet. Sci. Lett.*, *241*, 248–259, doi:10.1016/j.epsl.2005.10.020.

Ding, Z. L., J. M. Sun, S. L. Yang, and T. S. Liu (1998), Preliminary magnetostratigraphy of a thick eolian Red Clay–loess sequence at Lingtai, the Chinese Loess Plateau, *Geophys. Res. Lett.*, *25*, 1225–1228, doi:10.1029/98GL00836.

Ding, Z. L., E. Derbyshire, S. Y. Yang, Z. W. Yu, S. F. Xiong, and T. S. Liu (2002), Stacked 2.6-Ma grain size record from the Chinese loess based on five sections and correlation with the deep-sea δ^{18}O record, *Paleoceanography*, *17*(3), 1033, doi:10.1029/2001PA000725.

Evans, M. E., and F. Heller (1994), Magnetic enhancement and palaeoclimate: Study of a loess/palaeosol couplet across the Loess Plateau of China, *Geophys. J. Int.*, *117*, 257–264, doi:10.1111/j.1365-246X.1994.tb03316.x.

Evans, M. E., and F. Heller (2001), Magnetism of loess/paleosol sequences: Recent developments, *Earth Sci. Rev.*, *54*, 129–144, doi:10.1016/S0012-8252(01)00044-7.

Fang, X.-M., Y. Ono, H. Fukusawa, B.-T. Pan, J.-J. Li, D.-H. Guan, K. Oi, S. Tsukamoto, M. Torii, and T. Mishima (1999), Asian summer monsoon

instability during the past 60,000 years: Magnetic susceptibility and pedogenic evidence from the western Chinese Loess Plateau, *Earth Planet. Sci. Lett.*, *168*, 219–232, doi:10.1016/S0012-821X(99)00053-9.

France, D. E., and F. Oldfield (2000), Identifying goethite and hematite from rock magnetic measurements of soils and sediments, *J. Geophys. Res.*, *105*, 2781–2795, doi:10.1029/1999JB900304.

Freeman, R. (1986), Magnetic mineralogy of pelagic limestones, *Geophys. J. R. Astron. Soc.*, *85*, 433–452.

Gallet, S., B.-M. Jahn, and M. Torii (1996), Geochemical characterization of the Luochuan loess-paleosol sequence, China, and paleoclimatic implications, *Chem. Geol.*, *133*, 67–88, doi:10.1016/S0009-2541(96)00070-8.

Ge, J. Y., and Z. T. Guo (2008), A Miocene-Pliocene loess-soil sequence in the Western Qinling Mountain: Implications on the tectonics and paleomonsoon, paper presented at the PAGE Global Monsoon Symposium, Shanghai.

Gu, Z. Y., D. Lal, T. S. Liu, Z. T. Guo, J. Southon, and M. W. Caffee (1997), Weathering histories of Chinese loess deposits based on U-Th series nuclides and cosmogenic ^{10}Be, *Geochim. Cosmochim. Acta*, *61*, 5221–5231, doi:10.1016/S0016-7037(97)00313-X.

Guo, Z., T. Liu, N. Fedoroff, L. Wei, Z. Ding, N. Wu, H. Lu, W. Jiang, and Z. An (1998), Climate extremes in loess of China coupled with the strength of deep-water formation in the North Atlantic, *Global Planet. Change*, *18*, 113–128, doi:10.1016/S0921-8181(98)00010-1.

Guo, Z. T., S. Z. Peng, Q. Z. Hao, P. E. Biscaye, and T. S. Liu (2001), Origin of the Miocene-Pliocene Red-Earth formation at Xifeng in northern China and implications for paleoenvironments, *Palaeogeogr. Palaeoclimatol. Palaeoecol.*, *170*, 11–26, doi:10.1016/S0031-0182(01)00235-8.

Guo, Z. T., W. F. Ruddiman, Q. Z. Hao, H. B. Wu, Y. S. Qiao, R. X. Zhu, S. Z. Peng, J. J. Wei, B. Y. Yuan, and T. S. Liu (2002), Onset of Asian desertification by 22 Myr ago inferred from loess deposits in China, *Nature*, *416*, 159–163, doi:10.1038/416159a.

Guo, Z. T., et al. (2008), A major reorganization of Asian climate by the early Miocene, *Clim. Past*, *4*, 153–174.

Hao, Q. Z., and Z. T. Guo (2004), Magnetostratigraphy of a late Miocene-Pliocene loess-soil sequence in the western Loess Plateau in China, *Geophys. Res. Lett.*, *31*, L09209, doi:10.1029/2003GL019392.

Hao, Q. Z., and Z. T. Guo (2005), Spatial variations of magnetic susceptibility of Chinese loess for the last 600 kyr: Implications for monsoon evolution, *J. Geophys. Res.*, *110*, B12101, doi:10.1029/2005JB003765.

Hao, Q. Z., and Z. T. Guo (2007), Magnetostratigraphy of an early middle Miocene loess-soil sequence in the western Loess Plateau of China, *Geophys. Res. Lett.*, *34*, L18305, doi:10.1029/2007GL031162.

Hao, Q. Z., F. Oldfield, J. Bloemendal, and Z. T. Guo (2008a), The magnetic properties of loess and paleosol samples from the Chinese Loess Plateau spanning the last 22 million years, *Palaeogeogr. Palaeoclimatol. Palaeoecol.*, *260*, 389–404, doi:10.1016/j.palaeo.2007.11.010.

Hao, Q. Z., F. Oldfield, J. Bloemendal, and Z. T. Guo (2008b), Particle size separation and evidence for pedogenesis in samples from the Chinese Loess Plateau spanning the past 22 m.y., *Geology*, *36*, 727–730, doi:10.1130/G24940A.1.

Heller, F. (1978), Rockmagnetic studies of the Upper Jurassic limestones from southern Germany, *J. Geophys.*, *44*, 525–543.

Heller, F., and M. E. Evans (1995), Loess magnetism, *Rev. Geophys.*, *33*, 211–240, doi:10.1029/95RG00579.

Heller, F., and T.-S. Liu (1984), Magnetism of Chinese loess deposits, *Geophys. J. R. Astron. Soc.*, *77*, 125–141.

Ji, J. F., W. Balsam, and J. Chen (2001), Mineralogic and climatic interpretations of the Luochuan loess section (China) based on diffuse reflectance spectrophotometry, *Quat. Res.*, *56*, 23–30, doi:10.1006/qres.2001.2238.

Kukla, G., and Z. S. An (1989), Loess stratigraphy in central China, *Palaeogeogr. Palaeoclimatol. Palaeoecol.*, *72*, 203–225, doi:10.1016/0031-0182(89)90143-0.

Kukla, G. J., Z.-S. An, J. L. Melice, J. Gavin, and J.-L. Xiao (1990), Magnetic susceptibility record of Chinese loess, *Trans. R. Soc. Edinburgh*, *81*, 263–288.

Larrasoana, J. C., A. P. Roberts, E. J. Rohling, M. Winklhofer, and R. Wehausen (2003), Three million years of monsoon variability over the northern Sahara, *Clim. Dyn.*, *21*, 689–698, doi:10.1007/s00382-003-0355-z.

Liang, M. Y., Z. T. Guo, A. Kahmann, and F. Oldfield (2009), Geochemical characteristics of the Miocene eolian deposits in China: Their provenance and climate implications, *Geochem. Geophys. Geosyst.*, *10*, Q04004, doi:10.1029/2008GC002331.

Liu, J. F., Z. T. Guo, Q. Z. Hao, S. Z. Peng, Y. S. Qiao, B. Sun, and J. Y. Ge (2005), Magnetostratigraphy of the Miziwan Miocene eolian deposits in Qin'an County (Gansu Province) (in Chinese with English abstract), *Quat. Sci.*, *25*, 503–508.

Liu, Q., S. K. Banerjee, M. J. Jackson, R. Zhu, and Y. Pan (2002), A new method in mineral magnetism for the separation of weak antiferromagnetic signal from a strong ferrimagnetic background, *Geophys. Res. Lett.*, *29*(12), 1565, doi:10.1029/2002GL014699.

Liu, Q., M. J. Jackson, S. K. Banerjee, R. Zhu, Y. Pan, and F. Chen (2003), Determination of magnetic carriers of the characteristic remanent magnetization of Chinese loess by low-temperature demagnetization, *Earth Planet. Sci. Lett.*, *216*, 175–186, doi:10.1016/S0012-821X(03)00477-1.

Liu, Q., M. J. Jackson, Y. Yu, F. Chen, C. Deng, and R. Zhu (2004), Grain size distribution of pedogenic magnetic particles in Chinese loess/paleosols, *Geophys. Res. Lett.*, *31*, L22603, doi:10.1029/2004GL021090.

Liu, Q., C. Deng, J. Torrent, and R. Zhu (2007a), Review of recent developments in mineral magnetism of the Chinese loess, *Quat. Sci. Rev.*, *26*, 368–385, doi:10.1016/j.quascirev.2006.08.004.

Liu, Q., A. P. Roberts, J. Torrent, C. Horng, and J. C. Larrasoana (2007b), What do the HIRM and S-ratio really measure in environmental magnetism?, *Geochem. Geophys. Geosyst.*, *8*, Q09011, doi:10.1029/2007GC001717.

Liu, T. S. (1985), *Loess and the Environment*, 251 pp., China Ocean Press, Beijing.

Liu, X., T. Rolph, Z. An, and P. Hesse (2003), Paleoclimatic significance of magnetic properties on the Red Clay underlying the loess and paleosols in China, *Palaeogeogr. Palaeoclimatol. Palaeoecol.*, *199*, 153–166, doi:10.1016/S0031-0182(03)00504-2.

Lu, H. Y., X. Y. Wang, Z. S. An, X. D. Miao, H. B. Tan, R. X. Zhu, H. Z. Ma, Z. Li, and X. Y. Wang (2004), Geomorphologic evidence of phased uplift of the northeastern Qinghai-Tibet Plateau since 14 million years ago, *Sci. Chin. (Ser. D)*, *47*, 822–833.

Maher, B. A. (1998), Magnetic properties of modern soils and Quaternary loessic paleosols; paleoclimatic implications, *Palaeogeogr. Palaeoclimatol. Palaeoecol.*, *137*, 25–54, doi:10.1016/S0031-0182(97)00103-X.

Maher, B. A., and R. Thompson (1991), Mineral magnetic record of the Chinese loess and paleosols, *Geology*, *19*, 3–6, doi:10.1130/0091-7613(1991)019<0003:MMROTC>2.3.CO;2.

Maher, B. A., and R. Thompson (1999), *Quaternary Climates, Environments and Magnetism*, Cambridge Univ. Press, New York.

Maher, B. A., V. V. Karloukovski, and T. J. Mutch (2004), High-field remanence properties of synthetic and natural submicrometre hematites and goethites: Significance for environmental contexts, *Earth Planet. Sci. Lett.*, *226*, 491–505, doi:10.1016/j.epsl.2004.05.042.

Mehra, O. P., and M. L. Jackson (1960), Iron oxide removal from soils and clays by a dithionite-citrate system buffered with sodium bicarbonate, *Clays Clay Miner.*, *7*, 317–327, doi:10.1346/CCMN.1958.0070122.

Nie, J., J. W. King, and X. M. Fang (2007), Enhancement mechanisms of magnetic susceptibility in the Chinese red-clay sequence, *Geophys. Res. Lett.*, *34*, L19705, doi:10.1029/2007GL031430.

Oldfield, F. (1991), Environmental magnetism: A personal perspective, *Quat. Sci. Rev.*, *10*, 73–85, doi:10.1016/0277-3791(91)90031-O.

Oldfield, F., et al. (2003), A high resolution late Holocene palaeo environmental record from the central Adriatic Sea, *Quat. Sci. Rev.*, *22*, 319–342, doi:10.1016/S0277-3791(02)00088-4.

Oldfield, F., Q. Hao, J. Bloemendal, Z. Gibbs-Eggar, S. Patil, and Z. Guo (2009), Links between particle size and magnetic grain size: General observations and some implications for Chinese loess studies, *Sedimentology*, *56*, 2091–2106, doi:10.1111/j.1365-3091.2009.01071.x.

Peters, C., and M. J. Dekkers (2003), Selected room temperature magnetic parameters as a function of mineralogy, concentration and grain size, *Phys. Chem. Earth*, *28*, 659–667.

Sartori, M., M. E. Evans, F. Heller, A. Tsatskin, and J. M. Han (2005), The last glacial/interglacial cycle at two sites in the Chinese Loess Plateau: Mineral magnetic, grain-size and Be-10 measurements and estimates of palaeoprecipitation, *Palaeogeogr. Palaeoclimatol. Palaeoecol.*, *222*, 145–160, doi:10.1016/j.palaeo.2005.03.013.

Scheinost, A. C., A. Chavernas, V. Barron, and J. Torrent (1998), Use and limitations of second-derivative diffuse reflectance spectroscopy in the visible to near-infrared range to identify and quantify Fe oxide minerals in soils, *Clays Clay Miner.*, *46*, 528–536, doi:10.1346/CCMN.1998.0460506.

Sun, D. H., Z. S. An, J. Shaw, J. Bloemendal, and Y. B. Sun (1998), Magnetostratigraphy and palaeoclimatic significance of late tertiary aeolian sequences in the Chinese Loess Plateau, *Geophys. J. Int.*, *134*, 207–212, doi:10.1046/j.1365-246x.1998.00553.x.

Thompson, R., and F. Oldfield (1986), *Environmental Magnetism*, Allen and Unwin, London.

Torrent, J., and V. Barrón (2003), The visible diffuse reflectance spectrum in relation to the color and crystal properties of hematite, *Clays Clay Miner.*, *51*, 309–317, doi:10.1346/CCMN.2003.0510307.

Torrent, J., V. Barrón, and Q. S. Liu (2006), Magnetic enhancement is linked to and precedes hematite formation in aerobic soil, *Geophys. Res. Lett.*, *33*, L02401, doi:10.1029/2005GL024818.

Torrent, J., Q. S. Liu, J. Bloemendal, and V. Barrón (2007), Magnetic enhancement and iron oxides in the upper luochuan loess-paleosol sequence, Chinese Loess Plateau, *Soil Sci. Soc. Am. J.*, *71*, 1570–1578, doi:10.2136/sssaj2006.0328.

Walden, J., F. Oldfield, and J. P. Smith (1999), Environmental magnetism: A practical guide, *Tech. Guide 6*, Quat. Res. Assoc., London.

Zheng, H.-B., F. Oldfield, L. Yu, J. Shaw, and Z.-S. An (1991), The magnetic properties of particle-sized samples from the Luochuan loess section: Evidence for pedogenesis, *Phys. Earth Planet. Inter.*, *68*, 250–258, doi:10.1016/0031-9201(91)90044-I.

Zhou, L.-P., F. Oldfield, A. G. Wintle, S. G. Robinson, and J. T. Wang (1990), Partly pedogenic origin of magnetic variations in Chinese loess, *Nature*, *346*, 737–739, doi:10.1038/346737a0.

Zhu, R.-X., C. Laj, and A. Mazaud (1994), The Matuyama-Brunhes and Upper Jaramillo transitions recorded in a loess section at Weinan, north-central China, *Earth Planet. Sci. Lett.*, *125*, 143–158, doi:10.1016/0012-821X(94)90212-7.

J. Bloemendal and F. Oldfield, Department of Geography, University of Liverpool, Liverpool L69 7ZT, UK. (oldfield.f@gmail.com)

Z. Guo and Q. Hao, Key Laboratory of Cenozoic Geology and Environment, Institute of Geology and Geophysics, Chinese Academy of Sciences, Beijing 100029, China.

J. Torrent, Departamento de Ciencias y Recursos Agrícolas y Forestales, Universidad de Córdoba, Edificio C4, Campus de Rabanales, 14071 Córdoba, Spain.